JOURNAL OF COMPUTATIONAL PHYSICS 46, 271–308 (1982)

An Implicit Method for Electromagnetic Plasma Simulation in Two Dimensions*

J. U. BRACKBILL AND D. W. FORSLUND

Applied Theoretical Physics Division, Los Alamos National Laboratory, Los Alamos, New Mexico 87545

Received November 13, 1981

A new method for modeling low-frequency plasma phenomena is presented. The method uses an implicit formulation of the Vlasov–Maxwell equations to relax restrictions on the time-step and mesh spacing so that larger values which correspond to the frequencies and wavelengths of interest can be used. As a result, the range of length and time scales accessible to plasma simulation is increased by orders of magnitude. The algorithm, as embodied in a new code VENUS for electromagnetic plasmas in two dimensions, is described, its stability and accuracy analyzed through linear and nonlinear analysis, and its properties, including suppression of the finite grid instability, illustrated through its application to the Weibel instability.

INTRODUCTION

To extend the reach of nonrelativistic electromagnetic plasma simulation in two dimensions to longer physical length and time scales, an implicit method has been developed. The implicit method alters the way the coupled field and particle equations are advanced in time and eliminates many of the constraints on the time and space steps imposed by stability conditions.

As is well known, explicit formulations of the Vlasov–Maxwell equations are stable only for values of the time step Δt and mesh interval Δx that resolve all time and space scales [1, 2]. In electromagnetic plasma simulation, for example, one is required to use time steps which resolve light waves and space steps which resolve the Debye length, even when neither radiation nor charge separation effects are important. In many cases, the time and length intervals of interest are very large compared with the values of Δx and Δt that satisfy the stability conditions, and then many time and space steps are required to integrate over them. This prevents the application of explicit plasma simulation methods to many problems [3].

*This work was performed under the United States Department of Energy. The U.S. Government's right to retain a nonexclusive royalty-free license in and to the copyright covering this paper, for governmental purposes, is acknowledged.

0021-9991/82/050271-38$02.00/0

A number of algorithms have been developed to remove these restrictions. In some, the equations are split, as in one developed by Nielson and Lindman in which the field advancement algorithm is not subject to the Courant condition [4]. In others, reduced equations are formulated in which the fast time scales are eliminated. Two levels of reduction in two-dimensional, electromagnetic plasma simulation algorithms are the Darwin model, in which Maxwell's equations are solved in the nonrelativistic limit [5], and the Darwin model with fluid electrons, in which the electrons are modeled by a collisional, sometimes massless fluid [6–9]. In the Darwin formulation, light waves do not propagate and the corresponding limit $kc\,\Delta t < 2$ is replaced by the less restrictive condition, $\omega_{pe}\,\Delta t < 2$.

Even longer time intervals are accessible to hybrid models which eliminate the inertial response of the electrons and the corresponding limit $\omega_{pe}\,\Delta t$, where ω_{pe} is the electron plasma frequency. Of course, each reduced model describes a reduced range of physical phenomena.

It is the purpose of this paper to explore an alternative approach to modeling low-frequency electromagnetic phenomena in plasmas, namely, an implicit formulation of the equations. Many of the earlier difficulties in solving implicit equations described by Langdon [10], have been addressed by the recent work of Mason [11] and Denavit [12] on implicit moment methods, and more recently, the direct implicit methods developed by Friedman *et al.* [13].

In an implicit formulation, the restrictions on Δt are relaxed in a very different way. Instead of reducing the equations to eliminate the fast time scales, the full system of equations is differenced implicitly in the time variable and consequently made linearly stable for all Δt. In principle, Δt can assume any value. (In practice, nonlinearity and accuracy constraints limit Δt.) It can be chosen to resolve the time scale of interest, even when it does not resolve the highest mode. This property of implicit equations has been used in hydrodynamic and magnetohydrodynamic problems for some time [14–16].

It is argued here that the unresolved modes should be damped, and in this way removed from the problem. When this is done, the implicit formulation and the reduced equations are similar in their effect on unresolved time scales. Even when fast modes are damped, however, there can be important differences in the results between the two approaches. Consider, for example, Landau damping on the ion-acoustic time scale. This can be correctly represented by the solution of the implicit equations, but it is eliminated at the outset from the solutions of the hybrid model unless it is explicitly modeled [17]. Perhaps as important, the effect of unresolved modes on the solution can be measured simply by reducing the time step.

The method for solving the implicit equations applied here to electromagnetic plasmas in two dimensions is an extension of Mason's moment method [11]. His method for electrostatic plasmas in one dimension is based on the observation that particle and moment representations of the plasma do not differ significantly over one time step in their effect on the fields, because the fields depend only on the lowest two moments of the particle distribution, the charge density and current. Thus, implicitly formulated moment equations can be used to give stable estimates of the fields in

which particles move. Cumulative errors in the solution are reduced by reinitializing the moment equations each time step from the particle data, and by making the moment and particle descriptions as consistent as possible.

The application of this method to electromagnetic plasma simulation in two dimensions and an examination of its properties form the remainder of this paper.

The logical plan of the paper is as follows: The formulation of the implicit moment method for electromagnetic plasma simulation is described in Section 1. The fundamental equations are given, explicit and implicit methods are compared, and the implicit formulation is displayed. The numerical dispersion theory is developed in Section 2, especially as it relates to the linear and nonlinear stability of the implicit equations. An algorithm for the solution of the field equations and particle equations is outlined in Section 3. Comments on the similarities to the direct implicit method are made where appropriate [13, 18]. Finally, numerical results of a study of the nonlinear evolution of the Weibel instability are presented in Section 4 [1].

Throughout the discussion, appropriate spatial discretization is taken for granted, and the time discretization is emphasized (although an appendix giving a derivation of the moment equations is included). Coincidentally, one of the principal results of this work is that the implicit formulation also provides the means to suppress the finite grid instability when $\lambda_D/\Delta x \ll 1$ [19, 20]. (It is done differently than previously proposed in that it does not depend on altering the spatial differencing [21]. For discussion on this point, the attention of the reader is called to Section 2c and 4f.)

1. *Formulation of an Implicit Method for Electromagnetic Plasma Simulation*

Beginning with the fundamental equations describing the evolution of a plasma in an electromagnetic field, an implicit algorithm is formulated and the properties examined.

a. *Fundamental Equations*

The fundamental equations are Maxwell's equations

$$\frac{1}{c}\frac{\partial \mathbf{B}}{\partial t} + \nabla \times \mathbf{E} = 0, \tag{1.1}$$

$$\nabla \cdot \mathbf{B} = 0, \tag{1.2}$$

$$\frac{1}{c}\frac{\partial \mathbf{E}}{\partial t} - \nabla \times \boldsymbol{B} = -\frac{4\pi \mathbf{J}}{c}, \tag{1.3}$$

and

$$\nabla \cdot \mathbf{E} = 4\pi N, \tag{1.4}$$

where **E** is the electric field, **B** the magnetic induction, N the net charge density, and **J** the net current density; and the particle equations of motion

$$\begin{aligned} \frac{d\mathbf{x}_{sp}}{dt} &= \mathbf{u}_{sp}, \\ \frac{d\mathbf{u}_{sp}}{dt} &= \frac{q_s}{m_s}\left(\mathbf{E} + \frac{\mathbf{u}_{sp} \times \mathbf{B}}{c}\right), \end{aligned} \tag{1.5}$$

where s designates the particle type, and p the particle index.

Where $f_s(\mathbf{x}, \mathbf{u})$ is the distribution of particles of type s in $(\mathbf{x}, \mathbf{u})$, the net charge density and current are given by the moments of the distribution,

$$N = \sum_s N_s = \sum_s q_s \int f_s(\mathbf{x}, \mathbf{u})\, d\mathbf{u}$$

and

$$J = \sum_s J_s = \sum_s q_s \int d\mathbf{u}\, \mathbf{u} f_s(\mathbf{x}, \mathbf{u}).$$

b. *Plasma Simulation*

In the plasma simulation methods pioneered by Buneman and collaborators, [22], the large number of particles in a real plasma is represented by a relatively small number of simulation particles moving through a computation grid. With each particle is associated a position and a velocity (in addition to its charge and mass). In addition, each particle has a shape described by a shape factor h, a scalar function such that the definitions of charge and current on the grid for a numerical calculation are written [23, 24]

$$N_g = \sum_s q_s \sum_p h(\mathbf{x}_g - \mathbf{x}_{sp}) \tag{1.6}$$

and

$$\mathbf{J}_g = \sum_s q_s \sum_p \mathbf{u}_{sp} h(\mathbf{x}_g - \mathbf{x}_{sp}), \tag{1.7}$$

where g is the grid index. The shape factor h has the properties

$$1 = \int d\mathbf{x}\, h(\mathbf{x})$$

and

$$\begin{aligned} (\text{zone area})\, h(\mathbf{x}_g - \mathbf{x}'_g) &= 1, \qquad g = g', \\ &= 0, \qquad g \neq g'. \end{aligned} \tag{1.8}$$

With these definitions, the motion of the particles is reflected in changes in the field through N_g and $\mathbf{J}_g$, and, of course, vice versa.

c. *Explicit and Implicit Methods*

In an explicit plasma simulation method, the equations are marched in time with step Δt. To advance the solution from $n\,\Delta t$ to $(n+1)\,\Delta t$, the charge density and current are calculated from the particle data using Eqs. (1.6) and (1.7), the new fields are calculated using Eqs. (1.1)–(1.4), and finally the new particle velocity and position are calculated using Eqs. (1.5).

Exactly how the equations are solved has a profound effect on the accuracy and stability of the equations and much work has been done in this area, some of which is described in [2]. In general, though, all explicit methods are conditionally stable; that is, the time step must satisfy the inequality

$$\max_s \omega_{ps}\,\Delta t < 2,$$

where $\omega_{ps} = (4\pi n q_s^2/m_s)$ is the plasma frequency. It is to remove this constraint on Δt that we are lead to consider an implicit formulation of the equations.

In an implicit formulation, the solution is advanced from $n\,\Delta t$ to $(n+1)\,\Delta t$ by marching the equations backward from $(n+1)\,\Delta t$ to $n\,\Delta t$. The essential idea is that what would be numerically unstable solution with growth rate λ for $\Delta t > 0$ is also a numerically unstable solution with growth rate λ for $\Delta t < 0$. Since the solution is known at $n\,\Delta t$, however, the effect of solving the equations backwards to match this solution is to reduce the mode at $(n+t)\,\Delta t$ by the factor $\exp(-\lambda\,\Delta t)$ from its value at $n\,\Delta t$. Thus, the same difference equations which are unstable when solved forward can be stable when solved backward in time.

d. *Implicit Formulation*

Consider the implicit formulation of the equations with only time discretized, written

$$\frac{1}{c}(\mathbf{B}^{n+1} - \mathbf{B}^n) + (\nabla \times \mathbf{E}^{n+\theta})\,\Delta t = 0, \qquad \nabla \cdot \mathbf{B}^n = 0, \tag{1.9}$$

$$\frac{1}{c}(\mathbf{E}^{n+1} - \mathbf{E}^n) - \nabla \times \boldsymbol{B}^{n+\theta}\,\Delta t = -\frac{1}{c}\,4\pi \mathbf{J}^{n+\Gamma}\,\Delta t, \tag{1.10}$$

$$\nabla \cdot \mathbf{E}^{n+\theta} = 4\pi N^{n+\theta}, \tag{1.11}$$

$$\mathbf{x}_{sp}^{n+1} - \mathbf{x}_{sp}^{n} = \mathbf{u}_{sp}^{n+\theta}\,\Delta t, \tag{1.12}$$

and

$$\mathbf{u}_{sp}^{n+1} - \mathbf{u}_{sp}^{n} = \frac{q_s}{m_s}\left(\mathbf{E}^{n+\theta} + \frac{\mathbf{u}_{sp}^{n+\Gamma} \times \mathbf{B}^n}{c}\right)\Delta t, \tag{1.13}$$

where the superscript denotes the time at which the corresponding term is evaluated, and $0 \leqslant (\theta, \Gamma) \leqslant 1$. The field $\mathbf{E}^{n+\theta}$, for example,

$$\mathbf{E}^{n+\theta} = \theta \mathbf{E}^{n+1} + (1-\theta)\,\mathbf{E}^{n} \tag{1.14}$$

is a linear interpolate between $\mathbf{E}^{n+1}$ and $\mathbf{E}^{n}$. (In Eq. 1.13, $\mathbf{E}^{n+\theta}$ is evaluated at $\mathbf{x}_{sp}^{n+\Gamma}$. For all θ and $\Gamma > 0$, the equations are implicit. As θ and Γ increase from $\frac{1}{2}$ to 1, however, the formulation becomes more nearly backward differenced. When the equations are implicit, a coupled system of equations must be solved because unknown quantities, such as $\mathbf{B}^{n+\theta}$, appear on both sides of the equations. An iterative solution of Eqs. (1.9)–(1.13) is somewhat cumbersome, because each iteration requires solving the equations of motion for all the particles.

As Mason has observed [11], the information needed from the particles to advance the field is contained in the moments $N^{n+\theta}$ and $\mathbf{J}^{n+\Gamma}$, and these can be estimated by taking moments of the Vlasov equation. The resulting system of equations can be solved iteratively using methods similar to those used to solve the explicit equations.

The moment equations, however, can be derived more directly than from Vlasov's equation beginning with the definitions of $N^{n+\theta}$ and $\mathbf{J}^{n+\Gamma}$, written

$$N_s^{n+\theta} = q_s \sum_p h(\mathbf{x} - \mathbf{x}_{ps}^{n+\theta}), \tag{1.15}$$

and

$$\mathbf{J}_s^{n+\Gamma} = q_s \sum_p \mathbf{u}_{ps}^{n+\Gamma}\, h(\mathbf{x} - \mathbf{x}_{ps}^{n+\Gamma}). \tag{1.16}$$

As is shown in the Appendix, expansion of these equations yields moment equations (with particle equations of motion given by Eqs. (1.12) and (1.13)) which are written, neglecting all discrete grid effects,

$$N_s^{n+\theta} = N_s^{n} - \nabla \cdot \mathbf{J}_s^{n+\Gamma}\,(\theta\,\Delta t), \tag{1.17}$$

and

$$\mathbf{J}_s^{n+\Gamma} = \mathbf{J}_s^{n} - \nabla \cdot \mathbf{J}_s^{n+\Gamma}\,\mathbf{J}_s^{n}/N_s^{n} + \frac{q_s}{m_s}\left[N_s^{n+\Gamma}\mathbf{E}^{n+\theta} + \frac{\mathbf{J}_s^{n+\Gamma} \times \mathbf{B}^{n}}{c}\right](\Gamma\,\Delta t) - q_s \nabla \cdot \tilde{\mathsf{P}}_s(\Gamma\,\Delta t), \tag{1.18}$$

where N_s^{n} and $\mathbf{J}_s^{n}$ are calculated from the particle data using Eqs. (1.15) and (1.16) with $\theta, \Gamma = 0$, and $\tilde{\mathsf{P}}_s$ is the plasma pressure tensor defined by Eq. (A11).

It is appropriate to mention that the assumptions which are made in deriving the moment equations will impose an accuracy limit on the time step. The support of the moment equations derived in the Appendix is bounded by h to a cell and its eight nearest neighbors in two dimensions. To maintain the correspondence between moment and particle descriptions, it is necessary to bound the average particle

displacement to one cell per time step. When this limit is exceeded, as will be shown in the numerical results, energy conservation deteriorates.

The limitation on the time step is not fundamental to the moment method. Rather, it is a consequence of expanding Eqs. (1.15) and (1.16) about the particle positions at the beginning of the time step. If it were possible to guess the position of the particles to within one cell and expand Eqs. (1.15) and (1.16) about that position, the limitation would be removed. For example, an expansion about the free-streaming position of the particles,

$$\tilde{\mathbf{x}}_{ps} = \mathbf{x}_{ps}^{n} + \mathbf{u}_{ps}^{n}\,\Delta t,$$

is accurate so long as the action of the fields over a time step does not cause them to change cells [13]. In general, however, the turning points of the particle orbits complicate estimating $\tilde{\mathbf{x}}_{ps}$ for inhomogeneous or magnetized plasmas, and much work is necessary before reliable algorithms are developed. (This problem is addressed in [18].) When reliable estimates of particle positions are developed, modifying the moment equations to make use of the additional information is straightforward.

The equation for $\mathbf{J}_s^{n+\Gamma}$ can be written in the equivalent but more convenient form for computation,

$$\mathbf{J}_s^{n+\Gamma} = \hat{\mathbf{J}}_s + \frac{q_s}{m_s}\frac{(\hat{\mathbf{J}}_s \times \mathbf{B}^n)}{c}(\Gamma\Delta t) + \left(\frac{q_s}{m_s}\right)^2 \frac{(\hat{\mathbf{J}}_s \cdot \mathbf{B}^n)\,\mathbf{B}^n}{c^2}(\Gamma\Delta t)^2, \tag{1.19}$$

where $\hat{\mathbf{J}}_s$ is defined by

$$\hat{\mathbf{J}}_s = \Bigg[\mathbf{J}_s^n + \Bigg\{\frac{q_s}{m_s} N_s^{n+\Gamma} E^{n+\theta} - \nabla\cdot(\mathbf{J}_s^{n+\Gamma}\mathbf{J}_s^n/N_s^n) - \nabla\cdot\tilde{\mathbf{P}}_s\Bigg\}\Gamma\Delta t)\Bigg]/[1+(\omega_{cs}\Gamma\Delta t)^2], \tag{1.20}$$

and $\omega_{cs} \equiv q_s|\mathbf{B}|/m_s c$.

The pressure $\tilde{\mathsf{P}}_s$ must be approximated to close the equations. The choice of closure must reflect the need (a) to approximate the evolution of the particle moments as well as possible and (b) to construct a system of equations with favorable stability properties so that estimates of the fields can be made over long time intervals. Several choices are open without constructing an energy equation.

In the zero-temperature or cold-plasma limit, the pressure makes no contribution and thus the equations can be closed by the equation

$$\tilde{\mathsf{P}}_s = 0.$$

When $(k\lambda_D)^2 \ll 1$, the error made by neglecting $\tilde{\mathsf{P}}_s$ is small, and the moment equations are unconditionally stable.

To extend the method to warm plasmas, a more accurate $\tilde{\mathsf{P}}_s$ is needed. $\tilde{\mathsf{P}}_s$ can be approximated by its value at $n\,\Delta t$ as computed from the particle data,

$$\tilde{\mathsf{P}}_s = \mathsf{P}_s^n.$$

This approximation is appropriate when $(k\lambda_D)^2 = O(1)$, and is accurate to $O(\Delta t^2)$. Introduction of an explicit pressure, however, imposes a stability limit on the moment equations expressed by the inequality

$$(kC_s\,\Delta t) < 2\pi,$$

when $\theta = \Gamma = \frac{1}{2}$, where C_s is the adiabatic sound speed, $C_s^2 = dp/d\rho$ in the absence of thermal conduction. When the time-step inequality is expressed in terms of $(k\lambda_D)^2$,

$$(\omega_{pe}\,\Delta t)^2 < (2\pi)^2/(k\lambda_D)^2,$$

it is clear that the time step is restricted to the electron-plasma frequency time scale whenever $\tilde{\mathsf{P}}_s$ makes a significant contribution to the equation for the current. (Conversely, the spatial variation is limited to long wavelengths when $\omega_{pe}\,\Delta t$ is large.)

An implicit pressure formulation removes the stability limit on the time step, although the accuracy condition on the moment equations remains. One implicit pressure formulation can be derived by analyzing the pressure tensor $\mathbf{P}_s^n$ into a scalar pressure p_s^n defined by

$$(\nabla \cdot \nabla)\, p_s^n = \nabla \cdot (\nabla \cdot \mathbf{P}_s^n), \tag{1.21}$$

and a residual

$$\mathbf{Q}_s^n = \mathbf{P}_s^n - p_s^n 1. \tag{1.22}$$

A temperature can be defined from the equation of state

$$p_s^n = n_s^n k T_s^n, \tag{1.23}$$

where k is Boltzmann's constant. When the changes from t to $t + \Delta t$ occur isothermally, the scalar pressure can be advanced to $p_s^{n+\theta}$, where $p_s^{n+\theta}$ is given by

$$p_s^{n+\theta} = n_s^{n+\theta} k T_s^n. \tag{1.24}$$

With this substitution, the Courant limit imposed by the propagation of sound waves is effectively removed when the anisotropy in the pressure tensor is not too large. The consistency of the equations is not changed. For example, as will be shown the error in the energy is changed by terms of $O(\Delta t^2)$, the same order as the error caused by using $\nabla \cdot \mathbf{P}_s^n$ rather than $\nabla \cdot \mathbf{P}_s^{n+\Gamma}$.

With some assumption about $\tilde{\mathsf{P}}_s$, Eqs. (1.9)–(1.11), together with the continuity Eq. (1.17) and the current Eqs. (1.19) and (1.20) comprise a closed system which can be solved for $\mathbf{E}^{n+\theta}$ and $\mathbf{B}^{n+\theta}$. Because it is not necessary to recalculate the particle orbits each time the equations are iterated, the particles are moved just once each time step with considerable savings in computation time.

Although the particle simulation algorithm is emphasized, it is important to note that the formulation allows one or many species to be represented by the moment

equations alone. To convert the particle simulation to a hybrid model, all that is required is some prescription for the pressure. This may be as simple as an equation of state, or as complicated as an energy equation. Thus, the completeness of the description of the plasma given by the moment equations should be viewed as a positive aspect of the method, in that it increases the range of application enormously.

2. *Numerical Dispersion Theory*

a. *Linear Stability*

An obviously necessary condition for the stability of the implicit method is that the moment equations used to estimate the fields be linearly stable for large Δt. The linear stability is easily determined. Where the state variables are decomposed into constant and fluctuating parts and Fourier analyzed, the linearized equations corresponding to zero constant current and electric field, and a constant **B** field $\mathbf{B}_0$ can be written

$$0 = n_k^{n+\theta} - n_k^n + i\mathbf{k} \cdot \mathbf{j}_k^{n+\Gamma}(\theta \Delta t), \tag{2.1}$$

$$0 = \mathbf{j}_k^{n+\Gamma} - \mathbf{j}_k^n - \frac{q_s}{m_s}\left(n_0 \mathbf{E}_k^{n+\theta} + \frac{\mathbf{j}_k^{n+\Gamma} \times \mathbf{B}_0}{c}\right) \Gamma \Delta t + q_s i\mathbf{k} \cdot \mathbf{p}_k \Gamma \Delta t, \tag{2.2}$$

$$0 = \frac{1}{c}(\mathbf{B}_k^{n+\theta} - \mathbf{B}_k^n) + i(\mathbf{k} \times \mathbf{E}^{n+\theta})\,\theta \Delta t, \tag{2.3}$$

and

$$0 = \frac{1}{c}(\mathbf{E}_k^{n+\theta} - \mathbf{E}_k^n) - i(\mathbf{k} \times \boldsymbol{B}_k^{n+\theta})\,\theta \Delta t + \frac{1}{c} 4\pi \mathbf{j}_k^{n+\Gamma}\,\theta \Delta t. \tag{2.4}$$

When solutions of the form

$$\lambda n_k^n = n_k^{n+1} \tag{2.5}$$

are substituted into Eqs. (2.1)–(2.4), the roots of the resulting characteristic equation indicate whether the normal modes are amplified from time step to time step. For stability, the inequality

$$\lambda\lambda^* \leqslant 1 \tag{2.6}$$

must be satisfied.

The roots are calculated using standard eigenvalue routines [27]. The stability results can be summarized briefly. In the zero-temperature limit, the equations are unconditionally stable for $\theta, \Gamma \geqslant \frac{1}{2}$. For $\theta, \Gamma > \frac{1}{2}$, as θ, Γ or Δt increases, the value of $|\lambda|$ decreases to zero indicating damping. For $\theta, \Gamma = \frac{1}{2}$, $|\lambda|$ is exactly one for all values of Δt. In this special case, as Δt increases, λ tends toward -1.

TABLE I

Parameter	Value
c	1
a	0.025
ω_{pe}	1
ω_{pi}	0.1
B_0	0.1
m_e/m_i	0.01

If the temperature is not zero, the equations are stable for some range of Δt when $\theta, \Gamma > \frac{1}{2}$. Unconditional stability can be recovered if the pressure is made implicit, as may be done by assuming the equation of state

$$p^{n+1} = n^{n+1} k T^n. \tag{2.7}$$

With this substitution, the equations are once again stable for all Δt when $\theta, \Gamma \geqslant \frac{1}{2}$.

Information about the correspondence of the numerical and physical dispersion can be extracted from λ by equating $\exp[i(\omega + \gamma)\Delta t]$ to λ. A simple example illustrating this is shown in Figs. 1–3. The physical parameters for this example are given in Table I.

In Fig. 1, the variation of the real frequency with k, $0 \leqslant k\lambda_D \leqslant 1$, for $\theta = 0.6$, $\Gamma = \frac{1}{2}$ is shown. The time step, $\Delta t = 0.01\omega_{pe}^{-1}$, is small enough that even for $k = \lambda_D^{-1}$, $kc\,\Delta t$ is less than one. The modes from largest to smallest are light waves (right and left circularly polarized), electron-plasma oscillations, whistler waves, and ion-acoustic waves. In the figure, the smallest modes are indistinguishable from zero.

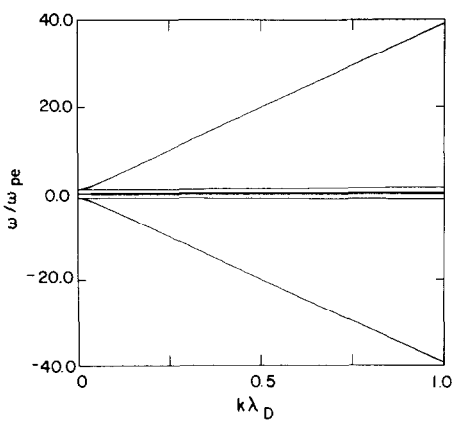

FIG. 1. The numerical dispersion curves for the moment equations are shown for wave propagation in the direction of the magnetic field. From the top, the curves represent light waves, electron-plasma oscillations, whistler and ion-acoustic waves. With $\Delta t = 0.01\,\omega_{pe}^{-1}$, physical frequencies are accurately reproduced.

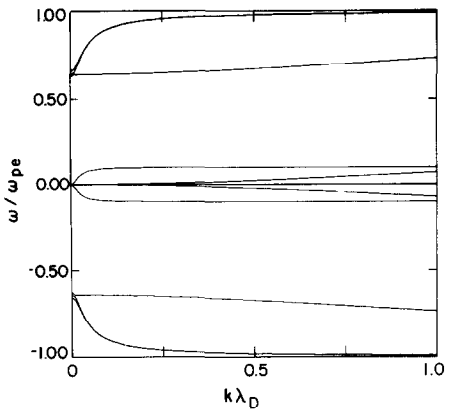

FIG. 2. For the same case as in Fig. 1 but with $\Delta t = \pi\omega_p^{-1}$, the numerical frequencies are compressed into the interval $-1 \leqslant \omega/\omega_p \leqslant 1$. From the top, the curves lie in the same order as in Fig. 1. The whistler and ion-acoustic frequencies are distinguishable and accurately reproduce the physical values, even though the frequencies of light waves and plasma oscillations are fractions of the physical values.

In Fig. 2, the variation of the real frequency with k is shown for the same case as in Fig. 1, but with $\Delta t = \pi\omega_{pe}^{-1}$. Now, the time step is large enough to introduce errors, and these are obvious. Quantitative comparisons are given in Table II where the shift in the real frequencies for $k\lambda_D = 1$ for large Δt relative to their value for small Δt are given. Evidently, when $\omega\,\Delta t$ is less than one there is an unambiguous correspondence between the physical (small Δt) and numerical (large Δt) values of the frequency. Furthermore, as $\omega\,\Delta t$ decreases below one, the correspondence improves very rapidly. For example, the whistler wave which asymptotes to the electron cyclotron frequency for large k is given within 1.4% for $\omega\,\Delta t = \pi/10$. From these results, one is lead to choose a Δt such that $\omega_{max}\,\Delta t < 1$, where ω_{max} is the maximum frequency of interest.

Because of the distortion of those modes for which $\omega\,\Delta t > 1$, the phase velocity of light waves decreases with increasing k. In fact, when $k\lambda_D = 1$, the phase velocity of a light wave is reduced by numerical error to a value equal to the electron thermal speed in the case shown in Fig. 2. As a consequence, one may expect to see the

TABLE II

Dispersion error with $\theta = 0.6$, $\Delta t = \pi$

Mode	$\omega\,\Delta t$	$\Delta\omega/\omega$	γ/ω
Light	40π	−0.975	0.130
Plasma	2π	−0.480	0.0727
Whistler	$\pi/10$	−0.0081	0.0002
Ion acoustic	$\pi/14$	−0.0041	0.0112

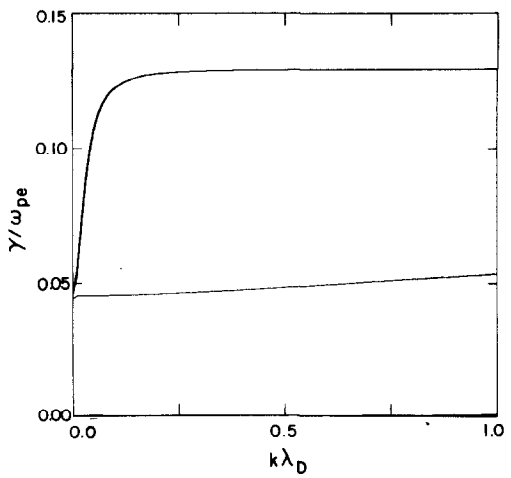

FIG. 3. The damping for $\Delta t = \pi$, $\theta = 0.6$ is shown. The curves are in the same order as in Fig. 2. Light waves and plasma oscillations are damped; the others are not.

Cerenkov instabilities studied by Godfrey [28, 29], in which resonant particles gain energy from the field but are unable to transfer it back. The numerical reduction of the phase velocity of light makes it likely that a very large portion of the plasma may become resonant with light waves to produce a disastrous instability.

When Δt is large, the unresolved waves are strongly damped as shown in Fig. 3 for $\theta = 0.6$, $\Gamma = 0.5$. For $k\lambda_D = 1$, the light waves are decremented by more than 10% each time step ($\gamma/\omega = 0.129$), and thus are virtually eliminated from a calculation. By contrast, the ion-acoustic mode is damped very little even for $k\lambda_D = 1$, as summarized in Table II. Of course, with larger values of θ, the damping may be unacceptably large [12].

The results shown in Table III for $k\lambda_D = 1$ indicate that the scaling of frequency

TABLE III

Scaling of dispersion with time step with $k\lambda_D = 1$

	Electron-plasma waves		Ion-acoustic waves	
Time step (ω_{pe}^{-1})	ω	γ/ω	ω	γ/ω
0.1	1.410	0.007	0.07080	0.00035
0.2	1.403	0.014	0.07080	0.00071
0.4	1.376	0.027	0.07079	0.0014
0.8	1.285	0.047	0.07078	0.0028
1.6	1.058	0.067	0.07072	0.0056
3.2	0.7255	0.073	0.07049	0.0112
6.4	0.4294	0.070	0.06961	0.022

errors and damping depends only on $\omega \Delta t$. For both electron-plasma and ion-acoustic waves, the damping scales linearly with $\omega \Delta t$ for a very wide range of time steps. Furthermore, for equal values of $\omega \Delta t$, the relative damping rates γ/ω are equal. Since the ratio of time and space steps is constant (as will be discussed in Section 2c), as Δt increases, the resolved wavelengths increase proportionately. In practice, the relative damping will remain constant, independent of Δt. Thus, while poorly resolved modes are strongly damped, well-resolved modes are not.

From observations such as these on the effect of implicit differencing, a simple, but effective, strategy for dealing with such problems emerges. The time step is chosen to resolve the fastest time scale of interest, and those modes not resolved by the time step are damped. This strategy is basically similar to that used in spatial differencing where smoothing through artificial viscosity or other means is added to ensure that the data remains resolvable by the grid. One difference between space and time discretization is that in space, all the data to be smoothed exists simultaneously. In time, it exists only at the present moment. Denavit has addressed this difficulty by storing several time levels to compute smoothing [12], but here the solution is interpolated between two time levels, one present and one future to obtain a qualitatively similar effect.

b. *Energy Conservation and Nonlinear Stability*

Linear stability analysis of the fluid equations reveals no difference in stability for finite Δt between the zero temperature and implicit pressure closure assumptions. Differences are seen when particle effects are included and the energy method is used [25]. The energy method associates stability with the boundedness of the solution in an appropriate norm. Here, the total energy integral is used as the norm in an analysis which includes $O(\Delta t^2)$ terms and particle effects in the limit $\Delta x = 0$, and is nonlinear in the field amplitudes.

As has been noted previously, energy is not a constant of the motion for leapfrog methods (except in the limit $\Delta t = 0$) because currents and forces at different times [29–31]. In the solution of the coupled fluid-field equations, however, it can be shown that energy does not increase over a time step in the zero temperature limit. Here, the particle contribution to the total energy is included and increases in energy over a time step (which correspond to instability) are shown to be associated with the closure assumption.

The total energy is the sum of the field and particle energies

$$W = \frac{1}{8\pi} \int (E^2 + B^2)\, dV + \sum_s \sum_p \tfrac{1}{2} m_s (u_{sp})^2. \tag{2.8}$$

The change in the total energy from time step to time step is of interest. Except for energy fluxes across the boundary, the numerical value of the total energy should be constant. If it is increasing, the increase is due to errors in the numerical algorithm which typically increase as λ_D increases. If it is decreasing, the numerical algorithm is stable but dissipative.

The change in the total energy is easily calculated. Consider first the field energy. The change in the field energy in a time step is

$$\Delta W_F = \frac{1}{4\pi} \int [\mathbf{E}^{n+1/2} \cdot (\mathbf{E}^{n+1} - \mathbf{E}^n) + \mathbf{B}^{n+1/2} \cdot (\mathbf{B}^{n+1} - \mathbf{B}^n)]\, dV. \tag{2.9}$$

Substituting from Eqs. (1.9) and (1.10) and noting that

$$\mathbf{E}^{n+\theta} = \mathbf{E}^{n+1/2} + (\theta - \tfrac{1}{2})(\mathbf{E}^{n+1} - \mathbf{E}^n), \tag{2.10}$$

and similarly for $\mathbf{B}^{n+\theta}$, ΔW_F can be written

$$\Delta W_F = \frac{c\,\Delta t}{4\pi} \int \nabla \cdot (\mathbf{E}^{n+\theta} \times \mathbf{B}^{n+\theta})\, dV - \Delta t \int (\mathbf{E}^{n+\theta} \cdot \tilde{\mathbf{J}}^{n+\Gamma})\, dV$$
$$- \frac{(\theta - \frac{1}{2})}{4\pi} \int [(\mathbf{E}^{n+1} - \mathbf{E}^n)^2 + (\mathbf{B}^{n+1} - \mathbf{B}^n)^2]\, dV. \tag{2.11}$$

The first term in Eq. (2.11) is the Poynting flux across the boundary of the domain. For an isolated system, its contribution is zero. The second term is the work done by the fields on the particles. The estimated current used to calculate the fields is denoted by $\tilde{\mathbf{J}}^{n+\Gamma}$. Whether it leads to an energy loss or gain is determined by comparing it with the energy gained by the particles from the fields. The third term represents a volume loss or gain of energy. Since the integral in this term is positive definite, the sign of the term depends on the sign of $(\theta - \frac{1}{2})$. For $\theta < \frac{1}{2}$, the contribution of this term is positive definite, the energy errors are positive and the numerical algorithm is unstable. For $\theta > \frac{1}{2}$, the contribution is negative definite, and the algorithm is stable but dissipative. Only for $\theta = \frac{1}{2}$ is the contribution identically zero.

The change in the particle energy can be evaluated similarly. The change in the particle energy is given by

$$\Delta W_p = \sum_s \sum_p m_s \mathbf{u}_{sp}^{n+1/2} \cdot (\mathbf{u}_s^{n+1} - \mathbf{u}_{sp}^n). \tag{2.12}$$

Once again, noting that

$$\mathbf{u}_{sp}^{n+1/2} = \mathbf{u}_{sp}^{n+\Gamma} + (\Gamma - \tfrac{1}{2})(\mathbf{u}_{sp}^{n+1} - \mathbf{u}_{sp}^n), \tag{2.13}$$

ΔW_p can be written

$$\Delta W_p = \sum_s \sum_p m_s \mathbf{u}_{sp}^{n+\Gamma} \cdot (\mathbf{u}_{sp}^{n+1} - \mathbf{u}_{sp}^n)$$
$$- (\Gamma - \tfrac{1}{2}) \sum_s \sum_p m_s (\mathbf{u}_{sp}^{n+1} - \mathbf{u}_{sp}^n)^2. \tag{2.14}$$

Once again, the second term is negative or zero only for $\Gamma \geqslant \frac{1}{2}$. Consistent with the

field energy result, the algorithm is stable with $\Gamma, \theta \geqslant \frac{1}{2}$. The first term represents the energy gained by the particles from the fields. Substituting from the equation of motion, Eq. (1.13), results in the equation

$$\sum_s \sum_p m_s \mathbf{u}_{sp}^{n+\Gamma} \cdot (\mathbf{u}_{sp}^{n+1} - \mathbf{u}_{sp}^{n}) = \sum_s q_s \sum_p (\mathbf{u}_{sp}^{n+\Gamma} \cdot \mathbf{E}^{n+\theta}) \Delta t = \mathbf{J}^{n+\Gamma} \cdot \mathbf{E}^{n+\theta} \Delta t \quad (2.15)$$

Collecting the appropriate terms one finds that the change in energy attributable to numerical error can be written

$$\begin{aligned} \Delta W = {} & \Delta t \int \mathbf{E}^{n+\theta} \cdot (\mathbf{J}^{n+\Gamma} - \tilde{\mathbf{J}}^{n+\Gamma})\, dV \\ & - \frac{(\theta - \frac{1}{2})}{4\pi} \int [(\mathbf{E}^{n+1} - \mathbf{E}^{n})^2 + (\mathbf{B}^{n+1} - \mathbf{B}^{n})^2]\, dV \\ & - (\Gamma - \tfrac{1}{2}) \sum_s m_s \sum_p (\mathbf{u}_{sp}^{n+1} - \mathbf{u}_{sp}^{n})^2. \end{aligned} \quad (2.16)$$

In magnetized plasmas (because of the gyrating motion of the particles), the last term in Eq. (2.16) will dominate ΔW. The effect will be to rapidly reduce the perpendicular temperature of the plasma to zero. To eliminate nonphysical cooling, Γ is always set to $\frac{1}{2}$ so that, in the absence of electric fields, the plasma kinetic energy is identically conserved. (One may have noted in Table II that the damping of the whistler wave was less than for the ion-acoustic wave, even though the whistler frequency is higher. The reason is that the whistler wave becomes the electron cyclotron wave for large k, and is thus undamped with $\Gamma = \frac{1}{2}$.)

The first term arises from the discrepancy between the particle and moment descriptions. It arises because the estimated current used to advance the fields may be different from the current which actually results from the action of the fields on the particles. The error can be computed by comparing the current computed from the moment equation, Eq. (1.18), and the current computed from the particles. Since the moment equation was derived by summing over particles, neglecting finite grid effects, the error arises from the estimate of the pressure $\tilde{\mathbf{P}}_s$. Therefore, the error in the energy transfer is given by

$$\begin{aligned} & \Delta t \int \mathbf{E}^{n+\theta} \cdot (\mathbf{J}^{n+\Gamma} - \tilde{\mathbf{J}}^{n+\Gamma})\, dV \\ & \quad = -\Gamma \Delta t^2 \sum_s q_s \int \mathbf{E}^{n+\theta} \cdot [\nabla \cdot (\mathbf{P}_s^{n+\theta} - \tilde{\mathbf{P}}_s)]\, dV. \end{aligned} \quad (2.17)$$

In general, the sign of the error is indefinite. If, however, the pressure is different from zero for only one specie (cold ions and hot electrons, for example) and that pressure is written

$$\mathbf{P}_s = 1(n_s k T_s), \quad (2.18)$$

then closing the moment equations by assuming $\tilde{\mathbf{P}}_s = 0$ leads to a positive definite volume error. Consider the volume term in the integral

$$\Delta t \int \mathbf{E}^{n+\theta} \cdot (\mathbf{J}^{n+\theta} - \tilde{\mathbf{J}}^{n+\theta})\, dV$$

$$= -\Delta t^2 q_s \int [\nabla \cdot (\mathbf{P}_s^{n+\theta} \cdot \mathbf{E}^{n+\theta}) - (\mathbf{P}_s^{n+\theta} \cdot \nabla) \cdot \mathbf{E}^{n+\theta}]\, dV. \tag{2.19}$$

Substituting from Eq. (1.11) yields

$$\Delta t^2 q_s \int (\mathbf{P}_s^{n+\theta} \cdot \nabla) \cdot \mathbf{E}^{n+\theta}\, dV = 4\pi \Delta t^2 q_s \int N_s^2\, kT_s\, dV > 0. \tag{2.20}$$

Thus, when the pressure term is neglected, the energy increases at a rate proportional to the plasma temperature. In other words, neglecting the pressure causes the equations to be nonlinearly unstable for $\theta = \frac{1}{2}$.

On the other hand, including the pressure explicitly causes the equations to be only conditionally stable for $\theta = \frac{1}{2}$. The Courant limit will not be restrictive in cases where $k\lambda_D \ll 1$. The restriction, however, arises in the fluid equations, and is removed by the assumption of an isothermal equation-of-state which allows one to make the pressure implicit as described earlier.

Because the equations are usually used with $\theta > \frac{1}{2}$, one might be concerned about energy losses due to numerical dissipation. The question is most easily answered by numerical experiments, but in the absence of mode coupling, poorly resolved modes are rapidly damped and cease to cause energy losses. Consider a particular mode ω of the system. The evolution of this mode is given by the amplification matrix

$$\mathbf{E}_\omega^{n+1} = \lambda_\omega \mathbf{E}_\omega^n = (\lambda_\omega)^n\, \mathbf{E}_\omega^0, \tag{2.21}$$

where $\mathbf{E}_\omega^0$ is the amplitude initially. The rate at which energy is lost from this mode between $n\,\Delta t$ and $(n+1)\,\Delta t$ is proportional to

$$\delta(\mathbf{E}_\omega)^2 = (\mathbf{E}_\omega^{n+1})^2 - (\mathbf{E}_\omega^n)^2 = (\lambda_\omega)^{2n}(\lambda_\omega - 1)^2 (\mathbf{E}_\omega^0)^2.$$

When λ_ω is small, as for poorly resolved modes ($\omega\,\Delta t > 1$), $\delta \mathbf{E}_\omega^2$ is small when n is sufficiently large.

With mode coupling, well-resolved modes can mode couple to produce modes at higher frequencies. These modes are more strongly damped because $(\gamma/\omega) \propto \omega$. One might, however, argue that energy losses are reduced because the higher frequencies are, at most, twice as large as the source frequencies in each mode coupling step. Thus, it requires several mode coupling steps to transfer energy from well-resolved modes to poorly resolved modes, a process which the increasing damping of intermediate modes would tend to suppress. That energy is conserved in numerical experiments tends to support this argument. (By comparison, if there were no damping for $\omega < \omega_0$ and heavy damping for $\omega > \omega_0$, energy transfer could occur in one step from undamped to damped modes and energy conservation may be poorer.)

c. *Plasma Dispersion Theory*

To illustrate the effect of the implicit formulation on the plasma dispersion theory, the dispersion relation for a one-dimensional, electrostatic plasma is developed. The dispersion theory is first developed in the limit $\Delta x = 0$, and later extended to include finite grid effects. (For convenience, it is also assumed that the number of particles in each element of phase space can be expressed as a distribution $f(x, v, t)$ and that the ions form a fixed, neutralizing background.)

In the usual way [26], Vlasov's equation is solved by the method of characteristics. Since $df/dt = 0$ along the particle orbits,

$$f(x^{n+1} - v^{n+\theta}\,\Delta t, v^{n+1} - q/mE^{n+\theta}\,\Delta t, t) = f(x^{n+1}, v^{n+1}, t + \Delta t), \tag{2.22}$$

where $0 \leqslant \theta \leqslant 1$ as before. Where $F_k(v)$ is the Fourier component of f, the Fourier component of the charge density is given by

$$N_k^n = q \int dv' F_k(v'), \tag{2.23}$$

the electric field is computed from estimated charge density at $(n + \theta)\,\Delta t$,

$$ikE_k^{n+\theta} = 4\pi \tilde{N}_k^{n+\theta},$$

and the time dependence is assumed,

$$f(x, v, t + \Delta t) = \exp(i\omega\,\Delta t)\,F(x, v, t),$$

the dispersion relation can be written

$$1 = \left(\frac{q^2}{m}\right)\left(\frac{\Delta t}{ik}\right)\frac{\tilde{N}_k^{n+\theta}}{N_k^n}\int dv' \frac{\partial F_0/\partial v'}{(\exp(-i(kv' - \omega)\,\Delta t) - 1)}. \tag{2.24}$$

In this equation, the integral is in standard form [26]. The only change is the coefficient $\tilde{N}_k^{n+\theta}/N_k^n$ which appears because the moment equations are used to solve for the electric field. The coefficient is given by the solution of the characteristic equation for the moment equations given above

$$\lambda = \tilde{N}_k^{n+\theta}/N_k^n. \tag{2.25}$$

Thus, to solve for the roots of the plasma dispersion equation, the roots of the moment equation for the corresponding case are first computed and substituted into Eq. (2.24), and the roots of the resulting relation are solved for in the standard way.

To extend this dispersion theory to include finite grid effects, one simply replaces ω_p^2 by $\lambda\omega_p^2$ in Eq. (35) in [26]. Particularly, since the finite grid instability, which has a growth rate of $O(\omega_{pe})$ has a potentially disastrous effect on long time-scale calculations, the effect of the dissipation in the formulation will be studied. As has

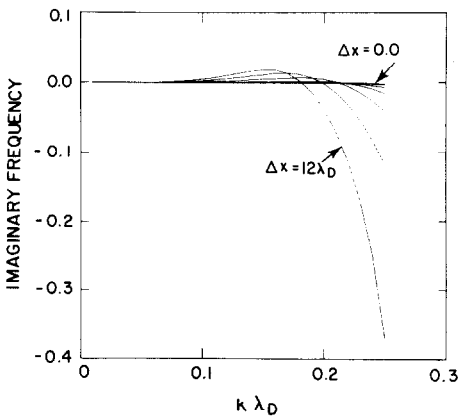

FIG. 4. The finite grid instability is unstable for $\Delta x > 0$. With $\Delta t = 0$, which corresponds to the result with an explicit formulation, the maximum growth rate is $0.025\omega_{pe}$.

been noted previously [12], the grid instability still occurs when an implicit formulation is used. The results given below, however, seem to suggest it can be suppressed by the numerical dissipation introduced by implicit time differencing.

First, because the instability is electrostatic, it is reasonable to assume that an analysis which includes electromagnetic effects would give similar results to one which does not. Beginning with Eq. (2.24), a dispersion relation which includes finite grid effects is obtained by combining a λ evaluated by substituting finite-difference approximations for spatial derivatives in the moment equations, with the form of the integral given by Lindman [26] which includes grid alias effects. For the electrostatic case, the solution for λ is elementary, and will not be discussed here. Similarly, the sum which replaces the integral in Eq. (2.24) when finite grid effects are included is given in [26]. The results for a finite grid unstable case are interesting, and are shown in Figs. 4 and 5. In Fig. 4, the imaginary part of the frequency, γ, is shown for a case

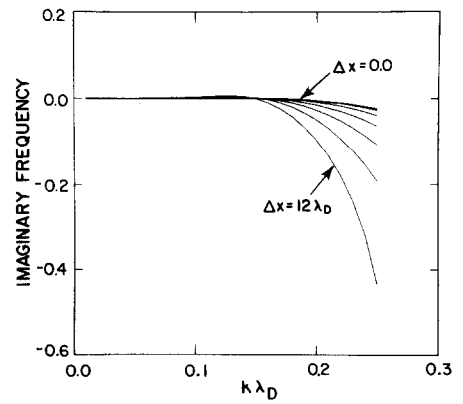

FIG. 5. The dispersion in the implicit moment equations reduces the finite grid instability. With $\omega_p \Delta t = 1$, the maximum growth rate is $10^{-3}\omega_{pe}$.

with $\omega_p \Delta t = 0$, $\theta = 1$. For $\Delta x = 12\lambda_D$, γ is positive corresponding to instability. With $\omega_p \Delta t = 1$ and $\theta = 1$, the maximum value of γ is reduced from $0.025\omega_{pe}$ to less than $10^{-3}\omega_{pe}$. Evidently, the effect of increasing the time step in the solution of the moment equations is to reduce the growth rate of the finite grid instability. As will be shown in the numerical results, the instability is also suppressed with $\omega_p \Delta t > 1$ and $\theta \simeq 0.6$.

The suppression of the finite grid instability by the numerical dispersion introduced by the moment equations is of considerable practical importance. It means that the quasi-neutral limit, where $\lambda_D/\Delta x \ll 1$ and $\omega_p \Delta t \gg 1$, is accessible to computation using the implicit moment method with sufficient dissipation.

The need to suppress the finite grid instability imposes a lower limit on the time step. The correspondence of the moment equations to the particles deteriorates when $v_{th} \Delta t/\Delta x$ is too large, and the finite grid instability occurs when it is too small. Empirically we take Δt satisfying the inequality

$$0(1) < v_{th}\Delta t/\Delta x \quad (\lambda_D/\Delta x)(\omega_p \Delta t) < 0(1), \tag{2.20}$$

the solutions are both stable and accurate.

Satisfying the inequality is not restrictive in practice. One notes that the conjunction of long-time and space scales is typical of most physical problems.

3. *An Algorithm for the Solution of the Implicit Equations*

a. *Potential Formulation*

The practice in the WAVE code [1, 32] has been followed in formulating the implicit field equations in a new code, VENUS, in terms of the scalar and vector potentials ϕ and $\mathbf{A}$ rather than $\mathbf{E}$ and $\mathbf{B}$ directly, although as Langdon has commented earlier, "In terms of the numerical and physical properties of the algorithms, there seem to be few grounds for preference either way..." [2]. Where $\mathbf{E}$ and $\mathbf{B}$ are given by

$$\mathbf{E} = -\nabla\phi - \frac{1}{c}\frac{\partial \mathbf{A}}{\partial t}, \tag{3.1}$$

and

$$\mathbf{B} = \nabla \times \mathbf{A}, \tag{3.2}$$

with the Coulomb gauge

$$\nabla \cdot \mathbf{A} = 0, \tag{3.3}$$

the homogeneous equations, Eqs. (1.1) and (1.2), are automatically satified. The inhomogeneous equations become

$$-\frac{1}{c^2}\frac{\partial^2 \mathbf{A}}{\partial t^2} + \nabla^2 \mathbf{A} = \frac{-4\pi \mathbf{J}}{c} + \frac{1}{c}\frac{\partial}{\partial t}(\nabla\phi) \tag{3.4}$$

and

$$\nabla^2\phi = -4\pi N. \tag{3.5}$$

It is the solution of Eqs. (3.4) and (3.5) with which the remainder of this section will be concerned.

b. *Consistency Requirements*

The spatial differencing of the field equations for WAVE has been discussed extensively elsewhere and will not be repeated [1, 2, 32]. However, the time differencing of the implicit equations raises several new issues. Specifically, one must choose the time levels in the equations consistent with both the difference equations (1.10) and (1.11) and the differential equations (3.4) and (3.5).

First, consistency with the difference equations requires that the same time levels appear on both sides of Eqs. (3.2) and (3.5),

$$\nabla^2\phi^{n+1} = -4\pi N^{n+1}, \tag{3.6}$$

and

$$\nabla \times \mathbf{A}^{n+1} = \mathbf{B}^{n+1}. \tag{3.7}$$

Second, the induction equation must be satisfied in difference form as well as in differential form,

$$\frac{1}{c}\nabla \times \left(\frac{\mathbf{A}^{n+1} - \mathbf{A}^n}{\Delta t}\right) + \nabla \times \left[\frac{1}{c}\left(\frac{\partial A}{\partial t}\right)^{n+\theta}\right] = 0, \tag{3.8}$$

or

$$\left(\frac{\partial \mathbf{A}}{\partial t}\right)^{n+\theta} = \frac{\mathbf{A}^{n+1} - \mathbf{A}^n}{\Delta t}. \tag{3.9}$$

Finally, as a consequence of choosing the Coulomb guage, the divergence of Eq. (2.4) satisfies

$$-4\pi\nabla \cdot \mathbf{J} + \frac{1}{c}\frac{\partial}{\partial t}(\nabla^2\phi) = 0 \tag{3.10}$$

If the solutions to the difference equations are also to satisfy $\nabla \cdot A = 0$, it follows from Eq. (3.10) and the continuity equation (1.17) that

$$\nabla^2\phi^{n+1} + 4\pi N^{n+1} = \nabla^2\phi^n + 4\pi N^n, \tag{3.11}$$

where N^n is the charge density appearing in Eq. (1.17); that is, the potential ϕ^n must be recalculated from the particle data at the beginning of each cycle rather than being carried over from the previous cycle. (There is no corresponding requirement for $\mathbf{A}^n$.)

Having assured consistency with the difference equations, we may now write down the potential equations to be solved,

$$-\frac{1}{c^2}\left(\frac{\mathbf{A}^{n+1}-2\mathbf{A}^n+\mathbf{A}^{n-1}}{\Delta t^2}\right)+\nabla^2\mathbf{A}^{n+\theta}=-\frac{4\pi\mathbf{J}^{n+\Gamma}}{c}+\frac{\nabla\phi^{n+1}-\nabla\phi^n}{\Delta t} \tag{3.12}$$

$$-\nabla^2\phi^{n+1}=4\pi N^{n+1}. \tag{3.13}$$

These equations, together with Eqs. (1.17) and (1.18), are solved each cycle to give the value of $\mathbf{E}^{n+\theta}$ needed to advance the solution.

c. *Iterative Solution of the Field Equations*

The solution of the field equations requires the simultaneous solution of the continuity, current, and potential equations. There are many ways to do this. Here, the method of Concus and Golub [34] is adapted as described by Nielson and Lewis [5]. The algorithm will differ in detail because the dependences on the unknown fields in Poisson's equation are different.

The goal in rewriting Eq. (1.11) is to obtain an equation for which the numerical operator to be inverted is diagonally dominant. To do this, the principal dependences on $\mathbf{E}^{n+\theta}$ on the *rhs* are identified and subtracted from both sides of the equation. The resulting equation is written

$$\nabla\cdot(1+\Omega)(\nabla\phi^{n+\theta})^{(l+1)}=4\pi(N^{n\theta})^{(l)}+\Omega(\nabla\phi^{n+\theta})^{(l)}, \tag{3.14}$$

where (l) denotes the iteration number and Ω and β are defined by

$$\Omega=\beta[1+\beta\omega_c^2\theta^2\,\Delta t^2/(1+\beta)] \tag{3.15}$$

and

$$\beta\equiv\Gamma\theta\omega_p^2\,\Delta t^2/(1+\theta^2\omega_c^2\,\Delta t^2). \tag{3.16}$$

The principal steps in the derivation of Eq. (3.14) are: Eq. (1.11) is rewritten

$$\nabla(\mathbf{E}^{n+\theta}-\mathbf{E}^n)=4\pi(N^{n+\theta}-N^n),$$

and $N^{n+\theta}-N^n$ is evaluated from Eq. (1.17). The current $\mathbf{J}^{n+\Gamma}$ in the resulting equation is evaluated from Eqs. (1.19) and (1.20), in which terms are rearranged so that the dependence on $\mathbf{E}^{n+\theta}$ is explicitly displayed,

$$\mathbf{J}^{n+\Gamma}=\hat{\hat{\mathbf{J}}}+\omega_p^2\left[\mathbf{E}^{n+\theta}+\frac{q}{m}\frac{\mathbf{E}^{n+\theta}\times\mathbf{B}^n}{c}(\Gamma\Delta t)+\left(\frac{q}{m}\right)^2\frac{(\mathbf{E}\cdot\mathbf{B})\,\mathbf{B}}{c^2}(\Gamma\Delta t)^2\right],$$

where $\hat{\hat{\mathbf{J}}}$ is defined by

$$\hat{\hat{\mathbf{J}}}\equiv\hat{\mathbf{J}}+\left(\frac{q}{m}\right)\frac{\hat{\mathbf{J}}\times\mathbf{B}^n}{c}(\Gamma\Delta t)+\left(\frac{q}{m}\right)^2\frac{(\hat{\mathbf{J}}\cdot\mathbf{B}^n)}{c^2}\mathbf{B}^n(\Gamma\Delta t)^2$$

and

$$\hat{\mathbf{J}} \equiv \mathbf{J}^n + [-\nabla \cdot (\mathbf{J}^{n+\Gamma}\mathbf{J}^n)/N^n - \nabla \cdot \tilde{\mathbf{P}}]\,\Gamma\Delta t/[1 + (\omega_c \Gamma \Delta t)^2].$$

Poisson's equation is now written

$$\begin{aligned}\nabla \cdot \mathbf{E}^{n+\theta} = \nabla \cdot [\mathbf{E}^n - 4\pi\hat{\hat{\mathbf{J}}}(\theta\Delta t)] \\ - \nabla \cdot \left\{\omega_p^2(\theta\Delta t)\left[\mathbf{E}^{n+\theta} + \left(\frac{q}{m}\right)\frac{\mathbf{E}^{n+\theta} \times \mathbf{B}^n}{C}(\Gamma\Delta t)\right.\right. \\ \left.\left. + \left(\frac{q}{m}\right)^2 \frac{(\mathbf{E}\cdot\mathbf{B})\mathbf{B}}{C^2}(\Gamma\Delta t)^2\right]\Big/[1 + (\omega_c\Gamma\Delta t)^2]\right\}\end{aligned}$$

Noting that Eq. (3.14) is an equation for the scalar potential, the transverse part of $\mathbf{E}^{n+\theta}$ is ignored, and the equation above can be solved for $\mathbf{E}^{n+\theta}$ in the same way Eq. (1.19) was derived from Eq. (1.18). Noting that $\mathbf{E}^{n+\theta} \cdot \mathbf{B}^n$ is proportional to $(\mathbf{E}^n - 4\pi\hat{\hat{\mathbf{J}}}(\theta\Delta t)) \cdot \mathbf{B}^n$, straightforward algebraic manipulation yields Eq. (3.14). To generalize Eq. (3.14) to multiple species, appropriate sums over species are taken in Eqs. (3.15) and (3.16).

(The equation for the potential is misleadingly reminiscent of the corresponding equation in the direct implicit method [13, 18]. The coefficient Ω is added only to maintain diagonal dominance, and is not the susceptibility.)

In solving for ϕ, Ω may be replaced by its average value over the mesh. For inhomogeneous plasmas, it is faster overall to solve for a pseudopotential,

$$\nabla\phi' = (1 + \Omega)\nabla\phi,$$

and solve a second potential equation to ensure zero circulation of the longitudinal field.

The equation for the vector potential, Eq. (2.10), is solved in a similar way. This time, however, terms of $O[(\omega_c\Delta t)^2]$ and higher are neglected. The resulting equation for $\mathbf{A}^{n+\theta}$ can be written in standard form

$$\begin{aligned}\left[\nabla^2\mathbf{A}^{n+\theta} - \frac{1}{\theta c^2\Delta t^2}(1 + \bar{\alpha}\Delta t)\mathbf{A}^{n+\theta}\right]^{(l+1)} \\ = -\frac{1}{c}4\pi\mathbf{J}^{n+\Gamma} + \frac{1}{\theta\Delta t}(\nabla\phi^{n+\theta} - \nabla\varphi^n) \\ - \bar{\alpha}\frac{\Delta t(\mathbf{A}^{n+\theta})^{(l)}}{\theta c^2\Delta t} + \frac{1}{\theta c^2\Delta t^2}[(1+\theta)\mathbf{A}^n - \theta\mathbf{A}^{n-1}],\end{aligned} \tag{3.17}$$

where $\bar{\alpha}(y)$ is the average of the maximum and minimum values of $\alpha(x, y)$ in x [5].

When the implicit pressure is used, the ω_p^2 appearing in Eq. (3.16) is replaced by $\omega_p^2 + k^2a^2$, where $k^2 \equiv 2/(2\pi)^2(1/\Delta x^2 + 1/\Delta y^2)$ and $a^2 = p^n/N^n$ is the "sound speed" as described earlier.

Experience has shown that the iteration converges with the equations described above, and the results of the previous cycle as the initial guess. The rate of convergence is adequate, but not remarkable. With $\omega_p \Delta t = 10$, the number of iterations required for a relative error of 10^{-5} is $O(10\text{–}20)$. (The convergence is not uniform, with very rapid convergence the first few iterations. This suggests that acceleration techniques might reduce the number of iterations substantially.)

d. *Solution of the Particle Equations of Motion*

After the fields have been estimated, the particle equations of motion (1.12) and (1.13) must be solved to complete the advancement of the solution from $n\Delta t$ to $(n+1)\Delta t$. As is noted in the Appendix, the equations of motion are written in the frame of the particle. The electric field $\mathbf{E}^{n+\theta}$ appearing in Eq. (1.12), for example, must be calculated at $\mathbf{x}^{n+\Gamma}$, the position of the particle at the intermediate time. When $\mathbf{E}^{n+\theta}(\mathbf{x}^{n+\Gamma})$ is obtained by interpolation from $\mathbf{E}^{n+\theta}(\mathbf{x}_g)$, Eqs. (1.12) and (1.13) form a system of polynomial equations for $\mathbf{x}^{n+\Gamma}$ and $\mathbf{u}^{n+\Gamma}$. To solve these equations, a simple Newton–Raphson iteration is used.

Note that Eq. (1.13) for $\mathbf{u}_{sp}^{n+1}$ can be written in the more convenient form

$$\mathbf{u}_{sp}^{n+\Gamma} = \left[\tilde{\mathbf{u}}_{sp} + \left(\frac{q_s}{m_s}\frac{\Gamma\Delta t}{c}\right)(\tilde{\mathbf{u}}_{sp} \times \mathbf{B}^n) + \left(\frac{q_s}{m_s}\frac{\Gamma\Delta t}{c}\right)^2 (\tilde{\mathbf{u}}_{sp}\cdot\mathbf{B}^n)\mathbf{B}^n\right]/(1+\omega_c^2\Gamma^2\Delta t^2), \tag{3.18}$$

where

$$\omega_x^2 \equiv \left(\frac{q_s}{m_s}\frac{\mathbf{B}^n}{c}\right)^2,$$

and the intermediate velocity $\tilde{\mathbf{u}}$ is given by

$$\tilde{\mathbf{u}} = \mathbf{u}^n + \frac{q_s}{m_s} E^{n+\theta}(\Gamma\Delta t). \tag{3.19}$$

In this form, the components of $\mathbf{u}^{n+\Gamma}$ are separated and the equations can be solved conveniently.

When the time step is large, the particle motion almost reduces to the guiding center limit,

$$\lim_{\Delta t\to\infty} \mathbf{u}_{sp}^{n+\Gamma} = \{(\mathbf{E}^{n+\theta} \times \mathbf{B}^n) + (\tilde{\mathbf{u}}_{sp}\cdot\mathbf{B}^n)\,\mathbf{B}^n\}/\mathbf{B}^n\cdot\mathbf{B}^n. \tag{3.20}$$

The $\nabla\mathbf{B}$ drifts are lost in this limit because the gyroradius contracts to zero with large time steps. When $\omega_c\Delta t < 1$, however, the $\nabla\mathbf{B}$ drifts are correctly represented even when the gyroradius is less than a cell because the exact particle orbits in the interpolated fields are calculated. (From the analysis given in [39], it appears that the correct fields are calculated even when $\nabla\mathbf{B}$ drifts are not, because the drift current is cancelled by the magnetization current.)

e. *Boundary Conditions*

The implicit formulation does not alter the treatment of boundary conditions significantly from that for explicit plasma simulation. (A complete description of boundary conditions is given, for example, in [2].) Some care must be taken with the solution of the particle equations of motion, because particles may leave the computational domain during the iteration. At present, periodic and aperiodic boundary conditions have been applied with no sensible difference in computational cost or difficulty.

4. *Numerical Results*

To illustrate the application of the implicit method to the calculation of a plasma instability, the results of simulation of the Weibel instability are presented [35]. This problem is chosen because numerical simulations exist to compare with [1], as well as some nonlinear theory [36], and it shows the behavior with larger time steps and cell sizes than were used in the calculations of magnetoacoustic shocks presented earlier [40]. The discussion will emphasize the numerical properties of the algorithm, namely, the effect of time and space discretization, closure assumptions, and centering on stability and energy conservation.

a. *The Weibel Instability*

The Weibel instability is driven by a temperature anisotropy in an unmagnetized plasma on an inductive time scale; that is, neither electrostatic plasma oscillations nor retardation effects alter the instability in any important way [37].

In a plasma characterized by an anisotropy a in the temperature in x and y, $a = (v_x^2/v_y^2 - 1)$, where v_x and v_y are the thermal velocities, the plasma instability is associated with a magnetic field $B_z(x)$ with mode structure $0 \leqslant k_x c/\omega_{pe} \leqslant a^{1/2}$ [1]

and decreases with decreasing values of a. Thus, as the growth of the instability decreases the anisotropy, the nonlinear evolution will be characterized by slower growth rates and the dominance of longer wavelength modes. The asymptotic value of a will be greater than zero for all finite periodic intervals.

b. *Numerical Simulation*

The evolution of a Weibel instability is displayed in Fig. 6, where the magnetic field energy is plotted for a simulation with $v_\perp/c = 0.1$, $a = 3$ and periodic intervals $0 \leqslant x \leqslant 10c/\omega_{pe}$, $0 \leqslant y \leqslant 20c/\omega_{pe}$. (Compared with the earlier calculations of Morse and Nielson [1], these have lower temperatures and anisotropies but similar periodic intervals.) The electric field energy is also plotted but is too small to be seen. The numerical parameters for the calculation are $\omega_{pe}\,\Delta t = 5$, $\theta = 0.55$, $N_x = 64$, $N_y = 32$. The pressure is implicit as described earlier.

As shown in Fig. 6, the magnetic field energy increases exponentially in the interval $0 \leqslant t \leqslant 350\omega_{pe}^{-1}$, at which time the instability saturates. Subsequent to

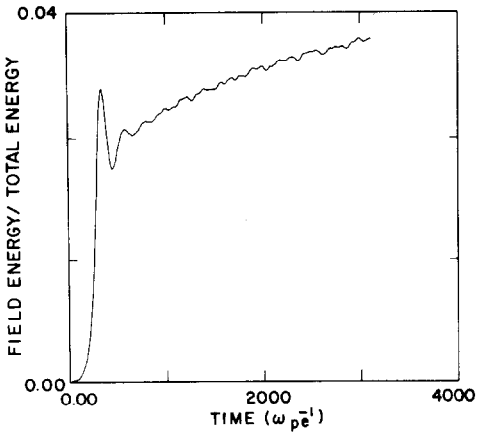

FIG. 6. The growth of the magnetic field energy due to the Weibel instability is shown. The energy remains high because the periodic interval is too small.

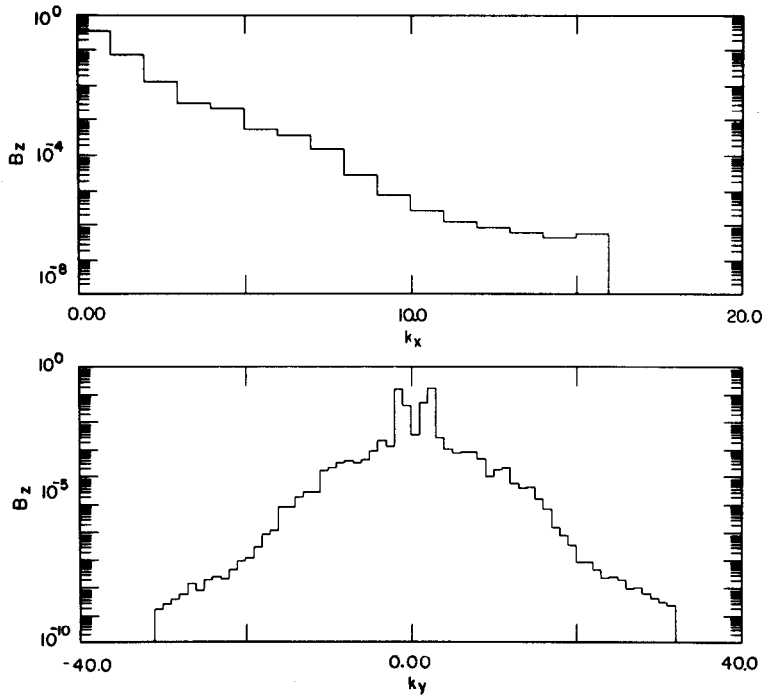

FIG. 7. Early in the growth of the Weibel instability, several modes in y are of comparable amplitude.

saturation, the energy continues to increase slowly until near the end of the calculation at $t = 3000\omega_{pe}^{-1}$. The slow growth can be approximated by the function

$$E_B(t) = E_\infty(1 - e^{-\lambda t}),$$

with $\lambda = 1/1500\omega_{pe}^{-1}$ and $E_\infty \equiv 3.0 \times 10^{-2}$.

The anisotropy a slowly decays to an asymptotic value greater than zero. The final value of a, $a = 0.62$, corresponds to a minimum unstable wavelength in y equal to $8.97c/\omega_{pe}$. Thus, only the longest representable wavelength is unstable, and only marginally so with the residual anisotropy.

The evolution of the spectrum can be seen by comparing the spectra of B_z at $t = 125\omega_{pe}^{-1}$ in Fig. 7 with that at $t = 3125\omega_{pe}^{-1}$ in Fig. 8. In both, those modes with $k_x = 0$ are largest. At the earlier time, the first two modes in k_y are large, but at the later time, only the first mode, the only unstable one, is still large.

The maximum value of the magnetic field energy can be compared with the nonlinear estimates [36]. From the nonlinear theory, the maximum relative value of the magnetic field energy is 5.6%. From the simulation, the observed maximum relative value is 5.13%.

As these results show, the numerical results of the calculation are consistent with

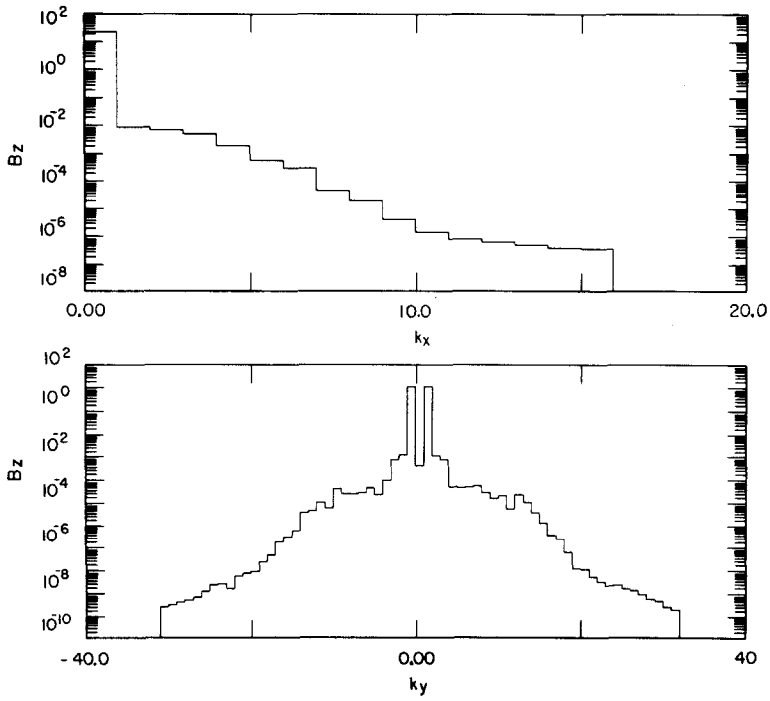

FIG. 8. Long after saturation of the instability, the longest wavelength mode is present and still very large.

linear and nonlinear theory, and, by extension, with the computational results [1]. There is, however, one significant difference. The time step, $\omega_{pe}\Delta t = 5$, is 25 times as large as that used in the earlier calculations, and the time interval represented is nearly 10 times as long.

The large time step may be expected to introduce some numerical error. For one thing, the rms displacement of a particle in y is 1.5 cells/time step. The errors do not appear to be unacceptably large, however. Only 8% of the total energy is lost over the course of the run.

c. *Implicit and Explicit Pressure*

Having established that the simulations correctly reproduce the physical behavior of the Weibel unstability, the discussion now focuses on numerical issues. First, the results when an explicit rather than an implicit pressure is used are considered.

In Fig. 9, the magnetic field energy history is plotted for a calculation with explicit pressure. The history can be divided into four intervals: exponential growth, saturation, decay, and finally, exponential regrowth. The first two correlate with the history shown in Fig. 6 with implicit pressure. The subsequent regrowth, however, occurs only with explicit pressure. Its cause is the heating of the plasma in the y direction leading to an actual change in sign of a. As the Weibel instability increases the temperature in y, a particle traveling at the thermal velocity in the y direction crosses more than one cell each time step. What is observed is that the rate of heating is proportional to the displacement, so that exponential instability results. The heating actually changes the sign of a, shown in Fig. 10, causing the magnetic field energy to increase again at the end of the calculation as a new Weibel instability grows with different polarization.

The observed instability is not the usual fluid instability, but it does occur when the Courant limit for stability of the moment equations is exceeded. The instability is

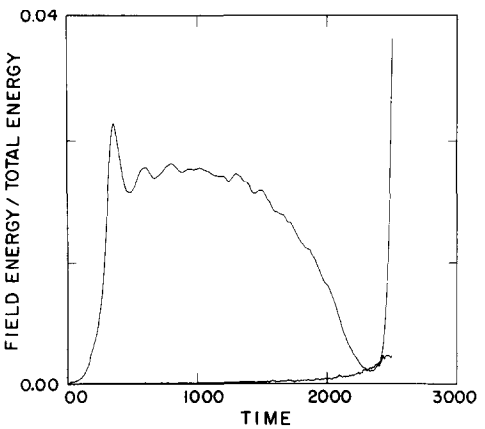

FIG. 9. With explicit pressure, the plasma is heated by a numerical instability which causes the magnetic field energy, shown here, to evolve differently than with implicit pressure (Fig. 6).

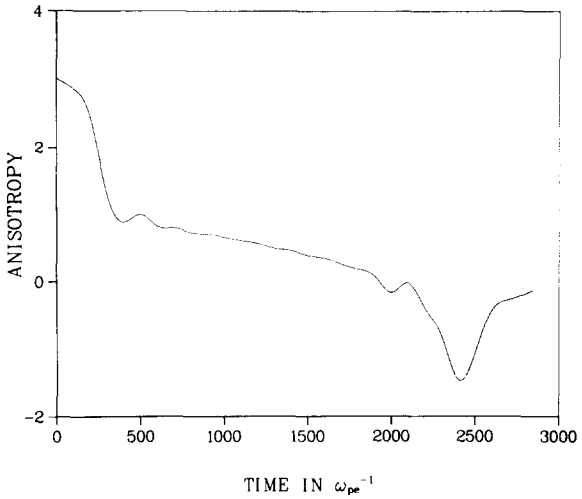

FIG. 10. With implicit pressure, the temperature anisotropy reverses sign causing the increase in magnetic field energy seen in Fig. 9.

probably altered by the reinitialization of the moment equations from the particle data each time step because coherent oscillations are washed out by fluctuations in the particle data. Nevertheless, the result is the same. When the Courant limit is exceeded with explicit pressure, significant heating (+ 900%) occurs (Fig. 9). With implicit pressure (Fig. 6), some dissipation occurs (−8%) which is larger than it would be were the time step smaller. Thus, the right-hand inequality in Eq. (2.28) does not represent a Courant limit for the implicit pressure formulation in the ordinary sense, since, when exceeded, it leads to only small increases in errors in energy conservation rather than instability.

d. *Long-Wavelength Results*

Because of the implicit formulation of the dynamical equations, the size of the periodic intervals can be increased without increasing the number of cells. In Figs. 11–13, the results are displayed for the same problem as that described earlier, but with $0 \leqslant x \leqslant 20c/\omega_{pe}$, and $0 \leqslant y \leqslant 40c/\omega_{pe}$, and $\omega_{pe}\,\Delta t = 10$. That is the periods are doubled in x and y, and the time step is doubled also at no increase in computational cost.

There are several interesting differences between the small and large "box" calculations, although clearly consistent with linear and nonlinear theory [36, 37]. First, the magnetic energy, shown in Fig. 11, decreases after saturation rather than continuing to increase, and it continues to decrease throughout the calculation. Second, the anisotropy a shown in Fig. 12, decreases to $a = 0.22$ at $t = 3000\omega_{pe}^{-1}$, much less than the value $a = 0.62$ observed in the small "box" case. The reason for these differences is simply that the larger box size increases the maximum representable wavelength and allows a closer approach to the final equilibrium values. Instead

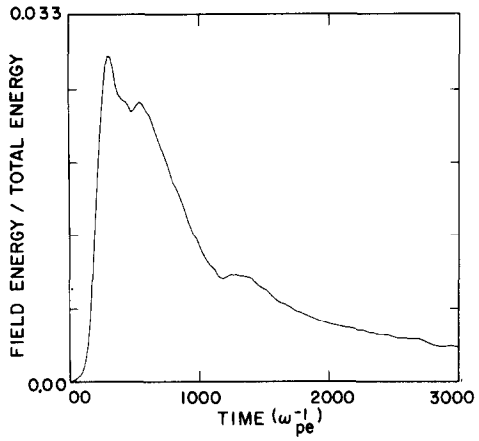

FIG. 11. With a larger periodic interval, the magnetic field energy decreases after saturation of the Weibel instability.

of the quasi-stationary result described earlier [1], we see the more typical decay of field energy as, for example, is often seen in electrostatic instabilities [38].

The steady state reached in the case of a small box has been described as a stationary magnetic *BGK* mode [1]. We see, however, from the simulation with a larger box that these modes are inherently unstable and dissipate if the system is large enough to allow coupling to longer wavelength Weibel modes.

This reasoning is supported by behavior of the spectrum shown in Fig. 13. At $t = 3000\omega_{pe}^{-1}$, only mode 1 is large, corresponding to the longest representable wavelength in the problem, $\lambda = 40c/\omega_{pe}$. This corresponds to a residual anisotropy of $a = 0.025$ compared with the observed value of $a = 0.223$. At this value, the first three modes in y are still unstable, but their growth times are much longer because a

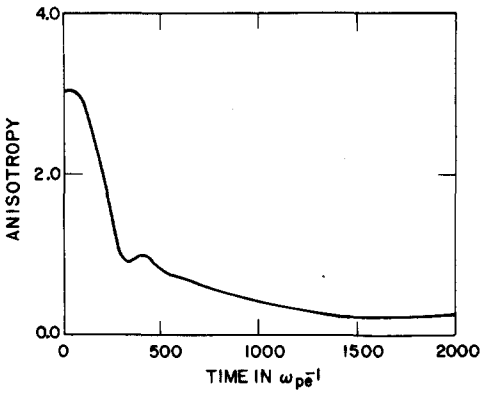

FIG. 12. The temperature anisotropy decays to a small fraction of its initial value due to the Weibel instability.

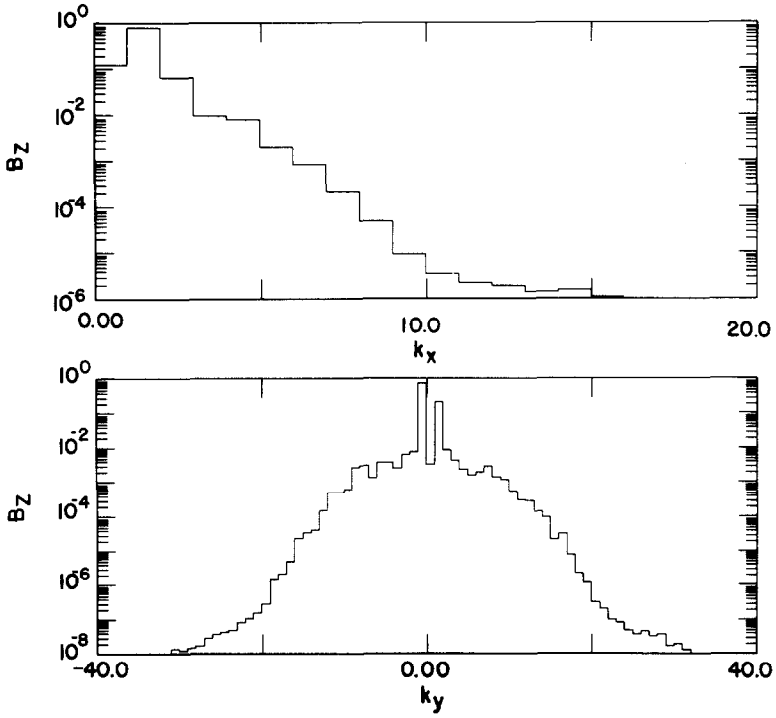

FIG. 13. Even with a larger box, only the longest wavelength mode in y is large indicating that the end state is always determined by the box size.

is small. Because of this, it may require a very long time for the asymptotic value of

e. *Energy Conservation*

The overall energy conservation gives a general measure of the accuracy of a calculation. Several numerical parameters can affect conservation, among them the time step, the number of particles, and the time-centering parameters θ.

The parameter θ has a special role, for its value is chosen to give the desired amount of dissipation. Over a narrow range, θ has been varied for the Weibel instability with explicit pressure and $\omega_{pe}\Delta t = 5$. Decreasing θ decreases the energy error proportionally for $\theta > \frac{1}{2}$. With $\theta = \frac{1}{2}$, however, the energy error is large, evidently as a result of the lack of selective dissipation to balance the heating introduced by the explicit pressure.

Changing the number of particles also affects the accuracy of the calculation. The small box case has been repeated with 22,500 particles rather than the 90,000 used above. The energy history is the same as before. The energy conservation, however, is much poorer. Almost 14% of the initial energy is lost compared with 4% with more

particles. With fewer particles, the electrostatic field energy is twice as large, and since it is probably the ultimate channel for energy loss, the energy loss is greater. With $\omega_{pe}\,\Delta t = 5$, the electrostatic fields are strongly damped to a level determined by sampling errors in the calculation of the charge density. Since the statistical error scales as $N^{-1/2}$, where N is the average number of particle per cell, fewer particles correspond to a higher field. It should be possible to estimate the proportionality constant between energy loss and particle number, but it has not been done.

f. *Finite Grid Instability*

Finally, the effect of making $\lambda_D/\Delta x$ small is considered. As is well known, when $\lambda_D/\Delta x \ll 1$, an instability due to aliasing errors on the spatial grid occurs [19, 20]. This instability has a nonzero growth rate even with $\Delta t = 0$, and saturates after heating the plasma until $\lambda_D/\Delta x = O(1)$. Because of these properties, its existence often determines the maximum meaningful time interval over which a plasma simulation can be continued.

In the implicit formulation of the equations, the finite grid instability has not been specifically addressed. Several properties of the implicit equations, however, mitigate the effects of the instability. For example, as Mason has described [11], simply increasing the time step suppresses the electric field and tends to reduce the growth rate of the instability. As evidence of this, the results shown in Fig. 14, with $\omega_{pe}\,\Delta t = 10$, can be compared with those in Fig. 15, with $\omega_{pe}\,\Delta t = 1$. In the latter, the jagged curve is the electric field energy. The results in Fig. 15 are clearly incorrect physically, for the total energy increases by to several times its initial value. The saturation of the instability is associated with an increase of $\lambda_D/\Delta x$ from 5.6×10^{-2}

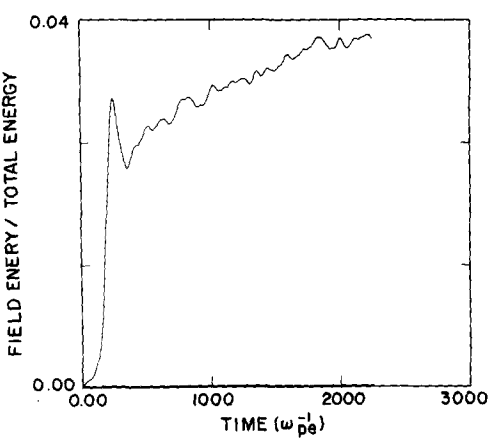

IG. 14. With a large time step, $\omega_{pe}\,\Delta t = 10$, the evolution of the Weibel instability is accurately esented even when $\lambda_D/\Delta x = 0.056$.

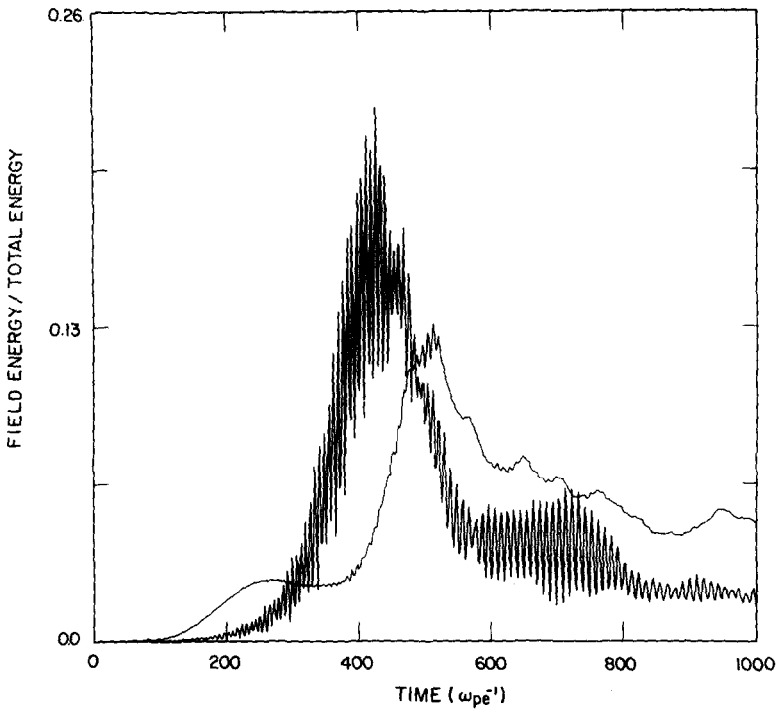

FIG. 15. With a small time step, $\omega_{pe}\Delta t = 1$, the finite grid instability dominates the evolution of the Weibel instability. A very large electric field (jagged curve) is generated and the plasma is heated until $\lambda_D/\Delta x \simeq 1$.

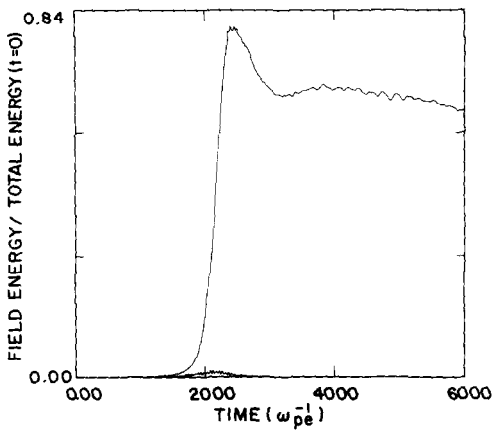

FIG. 16. Even with a large time step, $\omega_{pe}\Delta t = 10$, a finite grid instability results with a coarse grid $\lambda_D/\Delta x = 6 \times 10^{-3}$. With $\theta = 0.55$, the electric field due to numerical instability (which is just visible a $t = 2000\omega_{pe}^{-1}$) causes significant heating.

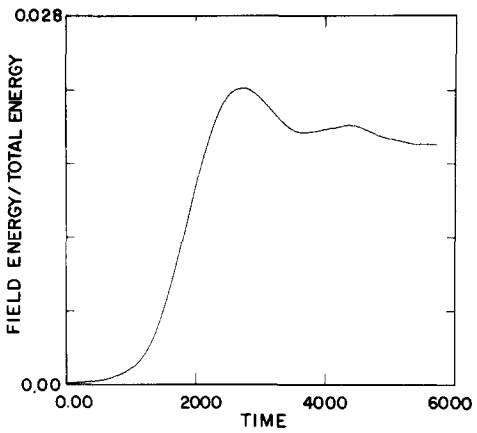

FIG. 17. When the dissipation is increased ($\theta = 0.8$), the finite grid instability is suppressed. The magnetic field energy is much smaller than in Fig. 16, and total energy conservation is excellent.

to approximately 5×10^{-1}. A comparison of the electric field energy E_E on the initial cycle indicates why reducing the time step increases the seriousness of the instability. With $\omega_{pe}\Delta t = 10$, $E_E = 5 \times 10^{-5}$, but with $\omega_{pe}\Delta t = 1$, $E_E \simeq 2 \times 10^{-3}$.

Even with $\omega_{pe}\Delta t = 10$, however, the instability can be troublesome. Results with $\lambda_D/\Delta x = 5.7 \times 10^{-3}$ are shown in Fig. 16. Although the electric field energy remains small compared with the magnetic field energy, the instability evidently causes an increase in the total energy by several hundred percent.

All is not hopeless, for, as has been described above, increasing the dissipation parameter θ reduces the growth rate of the finite grid instability. With $\lambda_D/\Delta x = 5.7 \times 10^{-3}$ and θ increased from the value 0.55 used to generate all previous results to $\theta = 0.8$, the results are as shown in Fig. 17. In this case, the measured growth time for the finite grid instability is $1.47 \times 10^5 \omega_{pe}^{-1}$, and the energy increases by 4% over the duration of the calculation. A higher value of θ would result in even longer growth times.

(It is possible that θ could be computed automatically. Perhaps θ can be recalculated from time to time, so that the change in total energy from cycle to cycle is small and slightly negative. Of course, for stability θ must be constrained to the interval, $\frac{1}{2} \leqslant \theta \leqslant 1$.)

CONCLUSIONS

An implicit plasma simulation algorithm for nonrelativistic, electromagnetic plasma simulation has been outlined, some of its numerical dispersion properties analyzed, and numerical results presented. From this discussion, it is apparent that the implicit formulation significantly extends the time and space scales accessible to plasma simulation. The increased capability is apparent in some of the problems

which have been studied using the VENUS code, among them the electromagnetic ion cyclotron [41], firehose, filamentation [41, K. Quest *et al.*, p. 1001; J. U. Brackbill and D. W. Forslund, p. 1010], and lower hybrid drift instabilities [41, J. U. Brackbill, p. 1046], and the study of enhanced lateral transport in laser irradiated plasmas [41, D. W. Forslund and J. U. Brackbill, p. 873]. The results will be presented at greater length at a later time.

It may not be as apparent that there are several ways in which using the implicit method differs from current practice in plasma simulation. With the implicit code, more time is spent solving the field equations than storing and fetching particles. This places greater emphasis on efficient calculation, and less on information transfer operations. It also seems to be true that fewer particles are required for a given problem. Evidently, the implicit formulation suppresses fluctuations, thereby reducing the noise level in the results. Finally, as well as an upper limit on the time step imposed by accuracy requirements, there appears to be a lower limit imposed by the need to suppress the finite grid instability as shown earlier.

There are many areas where more work is needed. Experience with the code has shown that more stable and accurate calculations of convective transport in the moment equations are necessary for strongly inhomogeneous plasmas. These can be carried over from ordinary fluid methods in a straightforward way. It is also straightforward to extend the plasma dispersion analysis to the electromagnetic case. Here the need may become apparent only after some unsuspected pathology.

Finally, there are obvious opportunities for extension of the method to new problem areas. Many problems could be done more easily using the moment equations in a hybrid description, especially when density variations are large or one component of the plasma is collisional. Also, it may be useful to extend the method to the guiding center model for application to strongly magnetized plasmas.

Clearly, the work presented here represents only the first step in exploiting the new opportunities offered by the implicit formulation.

APPENDIX: Derivation of the Moment Equations

Equations describing the evolution of the moments of the particle distributions can be derived directly beginning with the definitions of $N_s^{n+\theta}$ and $\mathbf{J}_s^{n+\Gamma}$. The definitions, written

$$N_s^{n+\theta} = q_s \sum_p h(\mathbf{x} - \mathbf{x}_{ps}^{n+\theta}) \tag{A1}$$

and

$$\mathbf{J}_s^{n+\Gamma} = q_s \sum_p \mathbf{u}_{ps}^{n+\Gamma} h(\mathbf{x} - \mathbf{x}_{ps}^{n+\Gamma}), \tag{A2}$$

are consistent with the representation of the plasma, but reduce to the ordinary definitions of charge and current density in the limit $\mathbf{x}_{g'} \to \mathbf{x}_g$, $g' \neq g$ (i.e., infinite

resolution). Our present interest is not in spatial discretization, but beginning with the definitions above has the advantage of removing all ambiguity concerning time discretization and identifies each of the terms in the equations with specific operations on the particle data.

Consider the definition for the charge density, Eq. (A1). From this definition, the continuity equation can be derived by expanding h about $\mathbf{x}_{ps}^n$, and using Eq. (1.12),

$$N_s^{n+\theta} = q_s \sum_p h(\mathbf{x} - \mathbf{x}_{ps}^n) - (\mathbf{u}_{ps}^{n+\Gamma}\, \theta\, \Delta t) \cdot \nabla h|_{\mathbf{x} \simeq \mathbf{x}_{ps}} + \cdots, \tag{A3}$$

where h is the piecewise linear function commonly used, the diffusionlike and higher-order terms are identically zero. Thus, substituting the definitions of charge and current density, Eqs. (1.6) and (1.7), yields the charge continuity equation

$$N_s^{n+\theta} = N_s^n - \nabla \cdot J_s^{n+\Gamma}\, \theta\, \Delta t. \tag{A4}$$

It is interesting to consider the nature of the discretization errors. For h other than piecewise linear, there are higher-order terms to consider. Further, when $\mathbf{u}_{ps}^{n+\Gamma}(\theta\,\Delta t)$ exceeds the support of h (i.e., $|\mathbf{u}_{ps}^{n+\Gamma}|\,\theta\,\Delta t > |\mathbf{x}_{p+1} - \mathbf{x}_{p-1}|$), the change in the charge

The equation for $\mathbf{J}_s^{n+\Gamma}$ is similarly derived by expansion. Substituting from the particle equation of motion, Eq. (1.13), Eq. (A2) can be written

$$\mathbf{J}_s^{n+\Gamma} = q_s \sum_p \mathbf{u}_s^n\, h(\mathbf{x} - \mathbf{x}_{ps}^{n+\Gamma}) + \frac{q_s^2}{m_s} \sum_p \left(\mathbf{E}^{n+\theta} + \frac{\mathbf{u}_{ps}^{n+\Gamma} \times \mathbf{B}^n}{c} \right) (\Gamma\, \Delta t)\, h(\mathbf{x} - \mathbf{x}_{ps}^{n+\Gamma}). \tag{A5}$$

Only in the first term in this equation is h expanded about $\mathbf{x}_{ps}^n$. Where a mean velocity is defined by

$$\bar{u}_s(\mathbf{x}) = \sum_p \mathbf{u}_{ps}\, \delta(\mathbf{x} - \mathbf{x}_{ps}) \Big/ \sum_p h(\mathbf{x} - \mathbf{x}_{ps}), \tag{A6}$$

and a fluctuating velocity by

$$\mathbf{u}'_{ps} = \mathbf{u}_{ps} - \bar{\mathbf{u}}_s(\mathbf{x}_{ps}), \tag{A7}$$

and where continuous particle density and currents are defined by

$$n_s(\mathbf{x}) = q_s \sum_p \delta(\mathbf{x} - \mathbf{x}_{ps}) \tag{A8}$$

and

$$\mathbf{j}_s(\mathbf{x}) = q_s \sum_p \mathbf{u}_{ps}\, \delta(\mathbf{x} - \mathbf{x}_{ps}), \tag{A9}$$

an equation for $\mathbf{J}_s^{n+\Gamma}$ accurate to first order in Δt can be written

$$\begin{aligned} J_s^{n+\theta} = \int d\mathbf{x}' \Bigg\{ \mathbf{j}_s^n - \left[\frac{\mathbf{j}_s^n}{n_s^n} (\nabla \cdot \mathbf{j}_s^{n+\Gamma}) + (\mathbf{j}_s^{n+\Gamma} \cdot \nabla) \frac{\mathbf{j}_s^n}{n_s^n} \right] \Gamma \Delta t \\ + \frac{q_s}{m_s} \left(n_s^{n+\Gamma} \mathbf{E}^{n+\theta} + \frac{\mathbf{j}_s^{n+\Gamma} \times \mathbf{B}^n}{c} \right) (\Gamma \Delta t) \Bigg\} h(\mathbf{x} - \mathbf{x}') \\ - q_s \nabla \cdot \tilde{\mathsf{P}}_s)(\Gamma \Delta t). \end{aligned} \tag{A10}$$

The last term in Eq. (A10) is the plasma pressure tensor

$$\tilde{\mathsf{P}}_s = \sum_p \mathbf{u}_{ps}'^n \mathbf{u}_{ps}'^{n+\Gamma}\, h(\mathbf{x} - \mathbf{x}_{ps}^n). \tag{A11}$$

about which more later.

When the moment equations are solved on a discrete mesh, variables such as $\mathbf{E}^{n+\theta}(\mathbf{x})$ are stored at mesh points and computed in between by interpolation,

$$\mathbf{E}(\mathbf{x}) = \sum_g \mathbf{E}_g\, h(\mathbf{x} - \mathbf{x}_g). \tag{A12}$$

When the support for h is bounded, nearby grid points are coupled together by the integral in Eq. (A10).

When the spatial domain is infinitely well resolved, however, the particle density and currents become equal to the grid density and current. For example,

$$\lim_{\mathbf{x}_{g'} \to \mathbf{x}_g,\, g' \neq g} \int d\mathbf{x}'\, n_s(\mathbf{x}')\, h(\mathbf{x} - \mathbf{x}') = N_s(\mathbf{x}). \tag{A13}$$

In this limit, the equation for $\mathbf{J}_s^{n+\Gamma}$ can be written

$$\begin{aligned} \mathbf{J}_s^{n+\Gamma} = \mathbf{J}_s^n - \nabla \cdot \mathbf{J}_s^n \mathbf{J}_s^{n+\Gamma} / N_s^n \\ + \frac{q_s}{m_s} \left[N_s^{n+\Gamma} \mathbf{E}^{n+\theta} + \frac{\mathbf{J}_s^{n+\Gamma} \times \mathbf{B}^n}{c} \right] (\Gamma \Delta t) - q_s \nabla \cdot \tilde{\mathsf{P}}_s. \end{aligned} \tag{A14}$$

Higher moments can be computed in a similar way. The moment equations, however, are truncated at $\mathbf{J}_s$, and the evolution of the pressure is obtained without solving an energy equation.

ACKNOWLEDGMENTS

Many intense and stimulating discussions with R. J. Mason, whose research motivated this work, are gratefully acknowledged. We also thank C. Nielson for very helpful criticism which pointed us in the right direction at the start, and helpful discussions with E. Lindman and D. C. Barnes.

REFERENCES

1. R. L. MORSE AND C. W. NIELSON, *Phys. Fluids* **14** (1971), 830.
2. A. B. LANGDON AND B. F. LASINSKI, *Methods Comput. Phys.* **16** (1976), 327.
3. D. WINSKE, *Phys. Fluids* **24** (1981), 1069.
4. C. W. NIELSON AND E. L. LINDMAN, *in* "Proceedings, 6th Conf. on Numerical Simulation of Plasmas, Lawrence Livermore Lab., Livermore, Calif.," Paper E3.
5. C. W. NIELSON AND H. R. LEWIS, *Methods Comput. Phys.* **16** (1976), 367.
6. J. BUSNARDO-NETO, P. L. PRITCHETT, A. T. LIN, AND J. M. DAWSON, *J. Comput. Phys.* **23** (1977), 300.
7. D. W. HEWETT AND C. W. NIELSON, *J. Comput. Phys.* **29** (1978), 219.
8. J. A. BYERS, B. J. COHEN, W. C. CONDIT, AND J. D. HANSON, *J. Comput. Phys.* **27** (1978), 363.
9. D. W. HEWETT, *J. Comput. Phys.* **38** (1980), 378.
10. A. B. LANGDON, *J. Comput. Phys.* **30** (1979), 202.
11. R. J. MASON, *J. Comput. Phys.* **47** (1981), 233; *Phys. Rev. Lett.* **41** (1981), 652.
12. J. DENAVIT, *J. Comput. Phys.* **42** (1981), 337.
13. A. FRIEDMAN, A. B. LANGDON, AND B. I. COHEN, *Comm. Plasma Phys. Contr. Fusion* **6** (1981), 225.
14. F. H. HARLOW AND A. A. AMSDEN, *J. Comput. Phys.* **8** (1971), 197.
15. C. W. HIRT, A. A. AMSDEN, AND J. L. COOK, *J. Comput. Phys.* **14** (1974), 227.
16. J. U. BRACKBILL, *Methods Comput. Phys.* **16** (1976), 1.
17. H. OKUDA, J. M. DAWSON, A. T. LIN, AND C. C. LIN, *Phys. Fluids* **21** (1978), 476.
18. D. C. BARNES AND T. KAMIMURA, "LOMEGA: A Low Frequency, Field Implicit Method for Plasma Simulation," Institute for Fusion Studies, Univ. of Texas, Austin, unpublished report.
19. A. B. LANGDON, *J. Comput. Phys.* **6** (1970), 247.
20. H. OKUDA, *J. Comput. Phys.* **10** (1972), 475.
21. L. CHEN, A. B. LANGDON, AND C. K. BIRDSALL, *J. Comput. Phys.* **14** (1974), 200.
22. O. BUNEMAN, *J. Comput. Phys.* **1** (1967), 517.
23. R. L. MORSE AND C. W. NIELSON, *Phys. Fluids* **12** (1969), 2418.
24. C. K. BIRDSALL AND D. FUSS, *J. Comput. Phys.* **3** (1969), 494.
25. R. D. RICHTMYER AND K. W. MORTON, "Difference Methods for Initial Value Problems," Interscience, New York, 1967.
26. E. L. LINDMAN, *J. Comput. Phys.* **5** (1970), 13.
27. B. T. SMITH, J. M. BOYLE, J. J. DONGARRA, B. S. GARBOW, Y. IKEBE, V. C. KLEMA, AND C. B. MOLER, "Matrix Eigensystem Routines—EISPACK Guide" (Lecture Notes in Computer Science, Vol. 6), Springer-Verlag, New York, 1976.
28. B. B. GODFREY, *J. Comput. Phys.* **15** (1974), 504.
29. B. B. GODFREY, *J. Comput. Phys.* **19** (1975), 58.
30. H. R. LEWIS, *J. Comput. Phys.* **6** (1970), 136.
31. A. B. LANGDON, *J. Comput. Phys.* **12** (1973), 247.
32. D. W. FORSLUND, "Plasma Simulation Techniques and Their Use," Los Alamos National Lab., unpublished report.
33. A. B. LANGDON, *Phys. Fluids* **15** (1972), 1149.
34. P. CONCUS AND G. H. GOLUB, *SIAM J. Numer. Anal.* **10** (1973), 1103.
35. E. S. WEIBEL, *Phys. Rev. Lett.* **2** (1959), 83.

36. D. S. LEMONS, D. WINSKE, AND S. P. GARY, *J. Plasma Phys.* **21** (1979), 287. D. S. LEMONS AND D. WINSKE, *ibid.* **23** (1980), 283.
37. G. KALMAN, C. MONTES, AND D. QUEMADA, *Phys. Fluids* **11** (1968), 1797.
38. D. W. FORSLUND AND C. R. SHONK, *Phys. Rev. Lett.* **25** (1970), 281.
39. C. L. LONGMIRE, "Elementary Plasma Physics," Wiley/Interscience, New York, 1963.
40. J. U. BRACKBILL AND D. W. FORSLUND, *Bull. Amer. Phys. Soc.* **25** (1980), 973.
41. K. LEE, J. U. BRACKBILL, D. W. FORSLUND, AND K. QUEST, *Bull. Amer. Phys. Soc.* **26** (1981), 920.